Gillen et al. Genome Biology (2021) 22:284
https://doi.org/10.1186/s13059-021-02494-w

Genome Biology

RESEARCH Open Access

Differential regulation of mRNA fate by the human Ccr4-Not complex is driven by coding sequence composition and mRNA localization

Sarah L. Gillen[1,2], Chiara Giacomelli[1], Kelly Hodge[1], Sara Zanivan[1,3], Martin Bushell[1,3*] and Ania Wilczynska[1,3*]

* Correspondence: martin.bushell@glasgow.ac.uk; awilcz@gmail.com
[1]Cancer Research UK Beatson Institute, Garscube Estate, Switchback Road, Glasgow G61 1BD, UK
Full list of author information is available at the end of the article

Abstract

Background: Regulation of protein output at the level of translation allows for a rapid adaptation to dynamic changes to the cell's requirements. This precise control of gene expression is achieved by complex and interlinked biochemical processes that modulate both the protein synthesis rate and stability of each individual mRNA. A major factor coordinating this regulation is the Ccr4-Not complex. Despite playing a role in most stages of the mRNA life cycle, no attempt has been made to take a global integrated view of how the Ccr4-Not complex affects gene expression.

Results: This study has taken a comprehensive approach to investigate post-transcriptional regulation mediated by the Ccr4-Not complex assessing steady-state mRNA levels, ribosome position, mRNA stability, and protein production transcriptome-wide. Depletion of the scaffold protein CNOT1 results in a global upregulation of mRNA stability and the preferential stabilization of mRNAs enriched for G/C-ending codons. We also uncover that mRNAs targeted to the ER for their translation have reduced translational efficiency when CNOT1 is depleted, specifically downstream of the signal sequence cleavage site. In contrast, translationally upregulated mRNAs are normally localized in p-bodies, contain disorder-promoting amino acids, and encode nuclear localized proteins. Finally, we identify ribosome pause sites that are resolved or induced by the depletion of CNOT1.

Conclusions: We define the key mRNA features that determine how the human Ccr4-Not complex differentially regulates mRNA fate and protein synthesis through a mechanism linked to codon composition, amino acid usage, and mRNA localization.

Introduction

The Ccr4-Not complex is a large evolutionarily conserved multi-protein complex [1–5], first described as a regulator of transcription [6–10]. It has since been shown to have key regulatory roles extending well beyond transcription. It is a major complex involved in regulating an mRNA throughout the entire mRNA life cycle including facilitating mRNA export [11], co-translational assembly of protein complexes [12],

translational repression [13, 14], deadenylation, and mRNA destabilization [15–17]. In humans, the Ccr4-Not complex has a molecular weight of ~ 1.2 MDa [18]. The details of how these different regulatory outputs are exerted and whether they are target-specific is not fully understood. At the heart of the Ccr4-Not complex is the CNOT1 subunit, one of the roles of this subunit is to function as a scaffold to bring together the complex subunits as well as many additional effector proteins contributing to the diverse functions of the complex and thus acts as the central node for all the complex's functions [16, 18–22].

The Ccr4-Not complex has been shown to be delivered to mRNAs by multiple different mechanisms including interaction with RNA-binding proteins that bind at the 3′ UTR [23–26], recruitment to miRNA-bound mRNAs by the miRISC complex [27] and interaction directly of the Not5 subunit with the E-site of ribosomes with no tRNA present at the A-site [28]. The most studied role of the Ccr4-Not complex is its involvement in mRNA deadenylation—the removal of the poly(A) at the 3′ end of the mRNA [29–32], which requires the activity of deadenylase subunits CNOT6/CNOT6L and CNOT7/CNOT8 (known as Ccr4 and Caf1, respectively, in yeast) [16, 33]. This is the primary event in the mRNA decay pathway followed by the removal of the 5′ cap and subsequent degradation of the target mRNA [27, 34–37]. Deadenylation requires the expulsion of the poly(A)-binding protein (PABP), which is thought to play an important role in the stability and translation of the mRNA [38].

The involvement of Ccr4-Not complex in the regulation of translation can be independent of its deadenylase activities [2]. Indeed, deadenylation is not essential for translation repression of an mRNA by the Ccr4-Not complex in conjunction either with RBPs [39, 40] or miRNAs [41–44]. Components of the Ccr4-Not complex are present in polysomes and are thought to be involved in translational quality control in yeast [45, 46]. In addition, the complex has been implicated as a player in the buffering of gene expression (mechanisms that allow for compensatory regulation of mRNA levels and translation in the maintenance of protein homeostasis) [47, 48].

The role of the open reading frame and its sequence composition has recently emerged as equally important in the control of gene expression as that of the 5′ and 3′ UTRs, which have traditionally been seen as the regulatory hubs of the mRNA. More specifically, codon usage has been highlighted as a key attribute linking translation elongation to mRNA stability [49–53]. Interestingly, it is the nucleotide at the third "wobble" position of the codon that can confer stabilizing / destabilizing effects on the mRNA [54]. The precise mechanisms linking codon usage to mRNA abundance, translation elongation, and protein output are still not fully understood.

It is clear that the Ccr4-Not complex is a master regulator of mRNA fate. Despite this, no effort has been made to uncouple the impact of the Ccr4-Not complex on translation and mRNA abundance in shaping the final proteome on a system-wide level. Also, there has not been a global investigation of the mRNA features that predispose an mRNA to specific fate outcomes regulated by the Ccr4-Not complex. Here we employed a number of high-throughput approaches—ribosome profiling, total RNA-seq, mRNA half-life studies, and pulsed SILAC—in the context of depletion of the scaffold protein CNOT1 to understand the complex's activity in post-transcriptional control. Knockdown of CNOT1 also downregulates the synthesis of many other subunits of the Ccr4-Not complex [19], which our results confirm (Additional File 1: Fig. S1A).

We identify the features of mRNAs that determine the mechanism by which the Ccr4-Not complex regulates mRNA fate. Specifically, we uncover the importance of the precise codon composition of an mRNA in determining how the Ccr4-Not complex controls mRNA stability. Moreover, we uncover that mRNA localization influences how the Ccr4-Not complex impacts mRNA translation: mRNAs translated at the ER are translationally downregulated after CNOT1 depletion, mRNAs that localize to p-bodies are translationally upregulated and mRNAs encoding proteins that localize to the nucleus are regulated at the level of translation but not stability by the Ccr4-Not complex. Lastly, we observe a role for the Ccr4-Not complex in the regulation of ribosome pause sites.

Results

Global increase of mRNA stability following CNOT1 knockdown

The Ccr4-Not complex is believed to be a major regulator of mRNA stability through its capacity to initiate mRNA decay by the deadenylase subunits, CNOT6/CNOT6L and CNOT7/CNOT8 [15, 17, 37, 55, 56]. Recruitment of the Ccr4-Not complex is thought to occur on all mRNAs at the end of the transcript lifecycle. It has been shown for specific mRNAs that decay can be accelerated by the presence of particular RNA motifs that are bound by RBPs which then interact with Ccr4-Not complex subunits [57–62]. However, this has not been tested on a global scale. To fully understand the distinct activities of the human Ccr4-Not complex in mRNA stability and translation, it was necessary to dissociate its roles in transcription from mRNA stability [2, 63], as both of these processes contribute to steady-state mRNA levels [64].

To determine how the Ccr4-Not complex impacts mRNA half-lives transcriptome-wide, we sampled RNA at multiple time points after transcriptional inhibition using triptolide [65] with and without CNOT1 depletion. Titration experiments were used to determine the optimal concentration of triptolide (1 μM), which produces a good decay curve for the short-lived MYC transcript without adversely affecting rRNA synthesis or cell viability (Additional File 1: Fig. S1B-D). RNA was isolated at 0, 0.5, 1, 2, 4, 8, and 16 h after transcriptional inhibition and the CNOT1 knockdown (Additional File 1: Fig. S1E) and RNA integrity (Additional File 1: Fig. S1F) were verified for each time point before performing RNA-seq.

Examination of RNA levels at each time point relative to the 0 h time point shows a global increase in mRNA stability following depletion of CNOT1 (Fig. 1A), clearly demonstrating the complex's central role in mRNA destabilization in human cells. An exponential model of decay $y \sim y_0\, e^{-kt}$ was fitted to the data, where k is the decay rate, y_0 is the mRNA level at time point 0, and y_t is the mRNA level at time t. The mRNA half-life was then calculated using the equation: $t_{1/2} = \ln(2)/k$. The half-lives obtained in control conditions for HEK293 cells showed a good correlation ($r = 0.406$) with published half-lives from HEK293 cells obtained using a 4-thiouridine-based methodology [66]. The median half-life in control conditions was 6.7 h, and there was an average log2FC in half-life of 2.1 following CNOT1 depletion (Additional file 2: Table S1), demonstrating there is a substantial global increase in mRNA stability. Using k-means clustering the mRNAs can be grouped into three major clusters that are distinguishable by their half-lives in the presence of CNOT1 and the extent of mRNA stabilization following CNOT1 depletion (Fig. 1B, C). This demonstrates that the vast majority of mRNAs

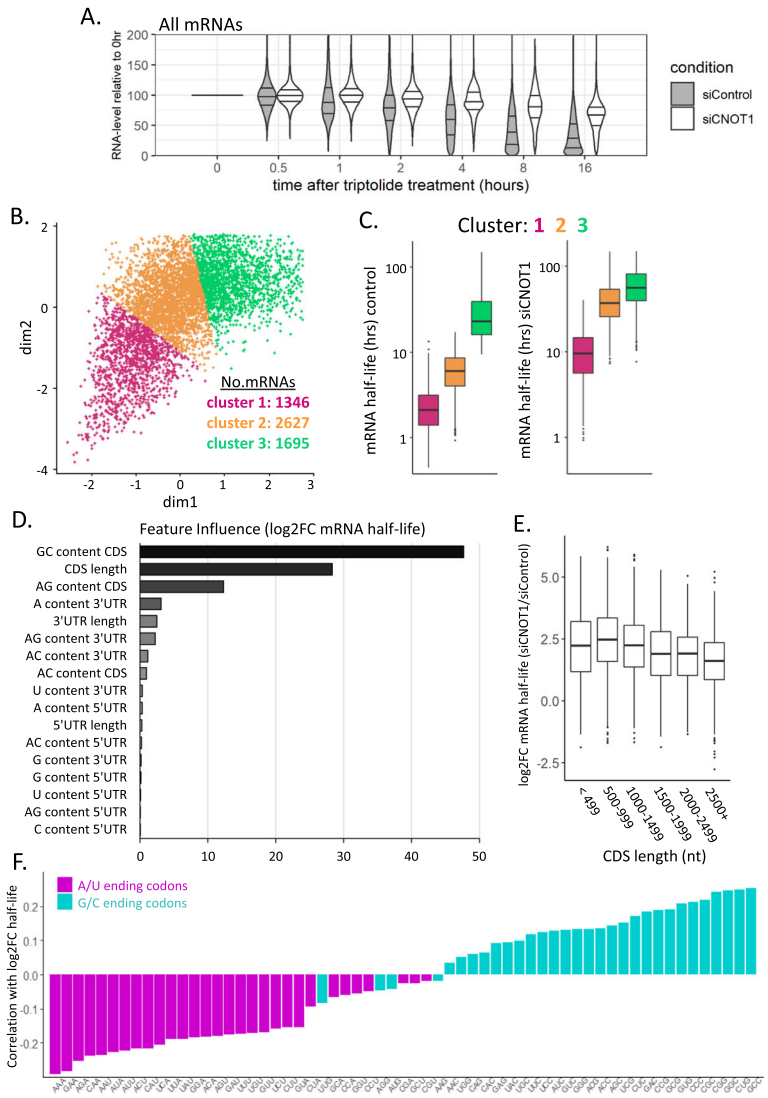

Fig. 1 G/C-ending codons drive mRNA destabilization by the Ccr4-Not complex. **A** Plot of RNA abundance across multiple time points after inhibition of transcription with triptolide relative to the 0 h timepoint for siControl and siCNOT1 treated samples (three biological replicates). **B** mRNAs grouped based on their mRNA half-life in the presence and absence of CNOT1 using k-means clustering. **C** The mRNA half-lives before and after CNOT1 depletion for the three major clusters of mRNAs determined in **B**. **D** The variable influence (determined using gradient boosting) of mRNA sequence features on the log2FC mRNA half-life after CNOT1 knockdown. **E** Log2FC mRNA half-life following CNOT1 depletion for mRNAs grouped by their CDS length. **F** Correlation coefficient (Spearman's rho) between the frequency of a given codon in an mRNA and the log2FC mRNA half-life (siCNOT1 / siControl). Codons with an A/U at the 3rd nucleotide position are colored in magenta and codons with a G/C at the 3rd nucleotide position are colored in cyan

rely on the Ccr4-Not complex for mRNA turnover and there are some mRNAs which are particularly susceptible to rapid destabilization by the Ccr4-Not complex. The mRNA half-lives for specific mRNAs from each cluster (Additional File 1: Fig. S2ABC) have been validated by qPCR with a different transcriptional inhibitor (flavopiridol) and a different pool of siRNAs targeting CNOT1 (Additional File 1: Fig. S2DEF). Overall, this shows that the Ccr4-Not complex is also the major regulator of mRNA stability in human cells and for the first time quantifies this on a global scale.

Moreover, gene ontology analysis conducted on all of the mRNAs ranked by their log2FC half-life after CNOT1 knockdown showed a significant enrichment for only a small number of terms, likely due to the fact that the Ccr4-Not complex is the major regulator of the stability of most mRNAs. The terms that were significant related to mitochondrion organization, cardiac/muscle development, and regulation of S/T kinase activity (Additional File 1: Fig. S3A). These observation may point toward a mechanism behind recent findings that the depletion of CNOT1 delays neurodevelopment [67] and affects cardiac function [68], in that, these specific subsets of mRNAs are heavily reliant on the Ccr4-Not complex for their stability.

G/C-ending codons drive Ccr4-Not-mediated mRNA destabilization

There are a number of attributes of the mRNA sequence that impact mRNA translation or stability including length, mRNA structure, and nucleotide composition within different regions of the mRNA [69, 70]. To determine if any of these are potentially involved in directing Ccr4-Not regulation of mRNA stability, the contribution of these variables to the change in mRNA half-life following CNOT1 knockdown was evaluated using gradient boosting [71]. First mRNA features were pre-filtered to remove highly correlated variables ($r > 0.7$, Additional File 1: Fig. S3B). Analysis of the independent variables showed that GC content and the length of the coding sequence (CDS) have the greatest influence on the change in mRNA half-life (Fig. 1D). Grouping of mRNAs by CDS length shows that shorter CDSes are associated with greater mRNA stabilization following CNOT1 knockdown (Fig. 1E).

The defining aspect of CDS sequence composition is that it is organized into codon triplets. CDS GC content is highly correlated with the GC content of the 3rd nucleotide of the codon (Additional File 1: Fig. S3C) and components of the Ccr4-Not complex have previously been implicated in codon-mediated regulation of mRNA translation in yeast and zebrafish [16, 28, 72]. Therefore, we hypothesized that the observed differences in human cells may be driven by the codon usage within the mRNAs.

The codon stabilization coefficient is the correlation between the codon frequency and the half-life of an mRNA [73]. Here we determined the correlation of the frequency of a given codon with the log2FC in mRNA half-life after CNOT1 depletion. Strikingly, this shows a strong split between the correlations of codon frequency of G/C-ending (cyan) and A/U-ending (magenta) codons with the change in mRNA half-life (Fig. 1F). In general, the greater the frequency of any given G/C-ending codon, the greater the increase in half-life after CNOT1 knockdown (Fig. 1F). Together, this supports the presence of G/C-ending codons is a primary driver of destabilization of an mRNA via the Ccr4-Not complex.

Synonymous codons are those which differ in sequence but encode the same amino acid. The distinct transcript pools present in proliferation and differentiation have been shown to have opposing synonymous codon usage signatures [74–76]. mRNAs enriched for A/U-ending codons are abundant in proliferation, whereas it is the mRNAs that contain more G/C-ending codons that are abundant in differentiation [75, 76]. Having observed a clear distinction in how G/C-ending and A/U-ending codons impact Ccr4-Not-mediated regulation of an mRNA's stability (Fig. 1F), we sought to understand if this was driven by synonymous codon usage differences. Hence, the

correlation of log2FC half-life with codon frequency (Fig. 1F) was reordered by the amino acid (Additional File 1: Fig.S3D). Unexpectedly, this highlights that while synonymous codons are important for the distinction of mRNA stability regulation by the Ccr4-Not complex, the amino acid itself further impacts the change in mRNA half-life with CNOT1 knockdown (Additional File 1: Fig. S3D). For example, the G/C-ending codons of some amino acids (e.g., Ala and Pro) correlate with an increase in mRNA stability, but their synonymous A/U-ending codons show very minimal correlation with stability changes (Additional File 1: Fig. S3D). A recent publication highlighted that amino acid composition also affects mRNA stability [77] and here we expand on this showing how amino acid differences contribute to the nature of the impact of G/C- or A/U-ending codons on mRNA stability regulation by the Ccr4-Not complex.

Translational regulation by the Ccr4-Not complex

It is proposed that the regulation of mRNA stability is linked to translation elongation [16, 52–54, 78, 79]. Recent structural data from yeast shows the Not5 subunit of the Ccr4-Not complex can interact directly with the ribosome; this interaction occurs at the ribosomal E-site when the A-site is unoccupied [28]. In addition to its described role in mRNA destabilization, the Ccr4-Not complex has also been implicated in the regulation of translational repression, which can occur independent of deadenylation [39, 41, 80–82]. As of yet, no study has investigated the role of the human Ccr4-Not complex at the level of translation on a system-wide level. Polysome gradients show there is a global accumulation of polysomes following CNOT1 depletion (Fig. 2AB). Whether the translational upregulation following CNOT1 depletion is a direct consequence of the global increase in mRNA stability (Fig. 1A) or if the role of the Ccr4-Not complex in the regulation of translation is distinct from how it controls mRNA stability is unknown. Therefore, to assess the impact of the Ccr4-Not complex on translation of individual mRNAs globally at codon resolution, ribosome profiling was conducted with and without the depletion of CNOT1 (Fig. 2AB, Additional File 1: Fig.S4A-C). Ribosome profiling involves high-throughput sequencing of ribosome-protected fragments (RPFs) [83, 84]. Quality control analysis of the RPF sequencing data showed the three replicates contained an extremely low number of reads aligning to rRNA (Additional File 1: Fig. S5A), were highly correlated (Additional File 1: Fig. S5B), had the expected read length distribution (Additional File 1: Fig. S5C), the majority of reads aligned to the CDS (Additional File 1: Fig. S5D), and showed a strong periodicity (Additional File 1: Fig. S5E). This demonstrates the ribosome profiling data is of very high quality and provides a benchmark ribosome profiling dataset.

Translational efficiency (TE) is defined as the number of RPFs aligning to a given CDS corrected for the mRNA's abundance (determined by parallel total RNA-seq). Due to differences in library preparation for RPFs and total RNA, differential expression analysis using DESeq2 [85, 86] was conducted separately for each library type to obtain a log2 fold change for RPF and RNA changes independently (Additional file 3: Table S2). The change in translational efficiency was then determined by calculating log2FC RPF – log2FC RNA. Our mRNA stability experiments demonstrated the global upregulation of mRNA stability after CNOT1 depletion (Fig. 1A). There is also a global increase in mRNA ribosome occupancy following CNOT1 depletion (Fig. 2B). Therefore,

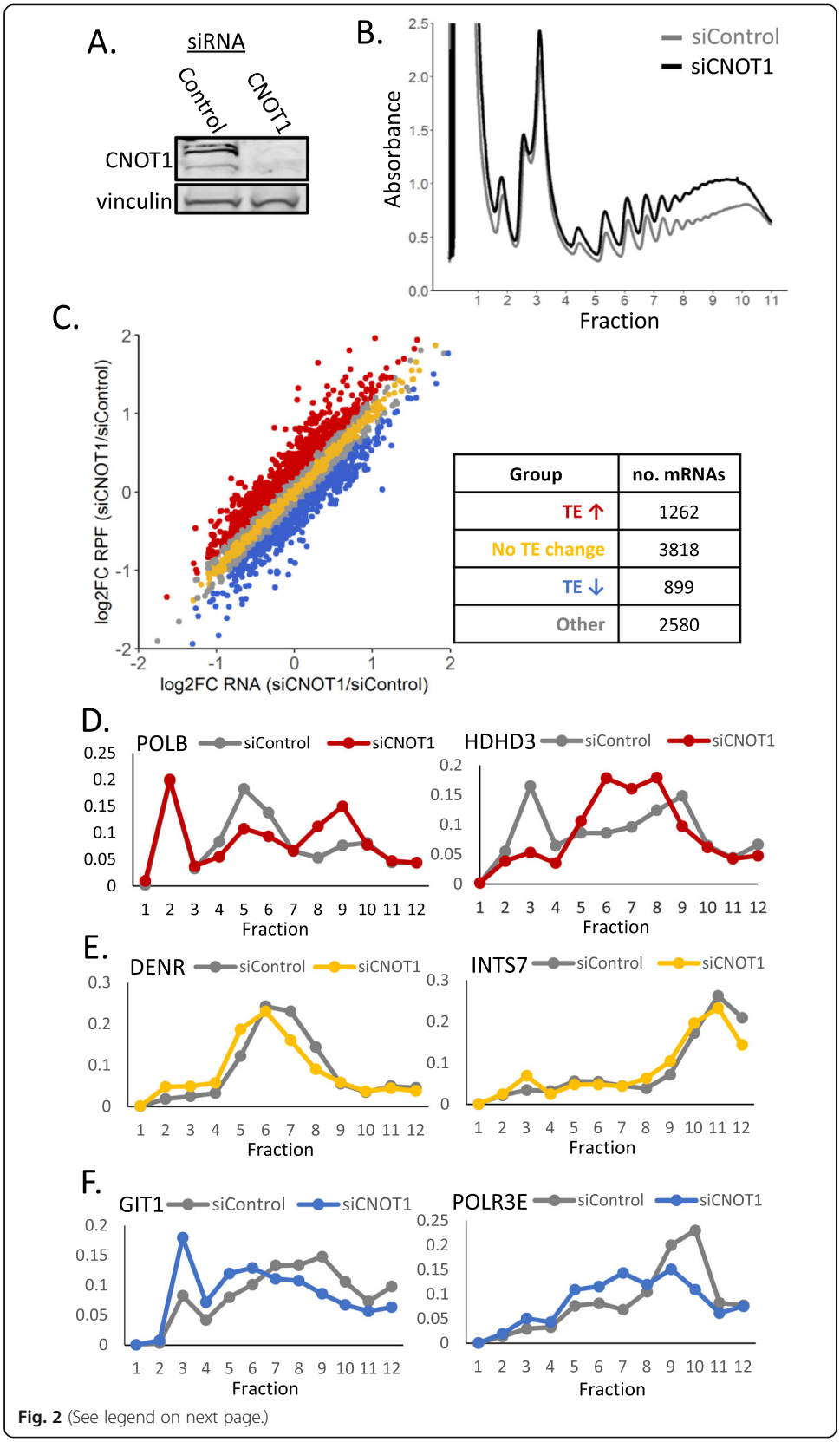

Fig. 2 (See legend on next page.)

(See figure on previous page.)
Fig. 2 Ribosome profiling identifies mRNAs regulated by the Ccr4-Not complex at the level of translation. **A** Western blot confirms siRNA knockdown of CNOT1. Vinculin is used as a loading control. **B** Polysome gradient profiles for samples treated with control or CNOT1-targeting siRNA. **C** There are groups of mRNAs with distinct changes in ribosome occupancy and mRNA abundance when CNOT1 is depleted. Log2 fold change of RPFs and RNA following CNOT1 depletion were determined using DESeq2 independently for each library type. Log2 translational efficiency (TE) was determined by log2FC RPF − log2FC RNA; a threshold of log2FC TE > 0.2 was used to categorize mRNAs as having increased TE and a log2FC TE < − 0.2 for mRNAs with decreased TE. No TE change was classified by a log2TE < 0.1 & > − 0.1. The table shows the number of mRNAs present in each group. **D–F** qPCR along gradient fractions from an independent experiment with and without CNOT1 depletion (n = 1 shown, n = 2 is shown in Additional File 1: Fig. S6). **D** Validation of the increased TE after CNOT1 depletion of POLB and HDHD3 from the group of mRNAs identified in (**C**) (red). In gray is the control and in red is the CNOT1 siRNA treated. **E** Validation of the unchanged TE after CNOT1 depletion for DENR and INTS7 from the group of mRNAs identified in (**C**) (yellow). In gray is the control and in yellow is the CNOT1 siRNA treated. **F** Validation of the decreased TE after CNOT1 depletion of GIT1 and POLR3E from the group of mRNAs identified in (C, blue). In gray is the control and in blue is the CNOT1 siRNA treated

in this condition, and due to the nature of differential expression analysis, it is more appropriate in this slightly unusual context to consider a negative log2FC as least upregulated and the positive log2FC as most upregulated. Using the ribosome profiling, three translationally regulated groups were defined (Fig. 2C): mRNAs with an increase in RPFs complementary to the increased mRNA stability thus having no effective TE change (yellow); mRNAs with a translation increase greater than the mRNA stability increase (increased TE; red) and mRNAs with a translational increase lower than the mRNA stability increase (decreased TE; blue). To validate the translational observations for individual mRNAs within these groups (Fig. 2D–F & Additional File 1: Fig. S6), independent experiments (n = 2) were conducted without cycloheximide pre-treatment, and RT-qPCR applied across all fractions of polysome gradients following treatment with CNOT1 or control siRNA. Using this alternative approach, we show that mRNAs with altered translational efficiency display the expected changes in polysome distribution (Fig. 2D, F, Additional File 1: Fig S6ABEF). In addition, mRNAs with correlated changes at both the RPF level and RNA level (no effective TE change, yellow) show no major changes in distribution across polysomes (Fig. 2E, Additional File 1: Fig. S6CD). Together this confirms the ribosome profiling analysis correctly identifies mRNAs with altered translation after CNOT1 knockdown.

Differentially translated mRNAs are functionally distinct

To determine if the functions of the proteins encoded by the mRNAs regulated at the level of translation by the Ccr4-Not complex are different, gene set enrichment analysis was conducted for the mRNAs ranked by the extent of the TE change with CNOT1 depletion (Fig. 3A, Additional File 1: Fig. S7AB, Additional file 4: Table S3). This showed a large number of gene ontology (GO) terms associated with decreased TE after CNOT1 knockdown. This included GO terms related to development and morphogenesis, cell signalling pathways and structural components of the cell (Additional File 1: Fig. S7A). These mRNAs are also associated with the endoplasmic reticulum (ER), extracellular matrix (ECM), and plasma membrane (Fig. 3A). To investigate this in more detail, cell lysates were separated into cytosolic and ER fractions (Fig. 3B) and the RNA present in each fraction sequenced. K-means clustering has been used to define mRNAs that predominantly localized to the cytosol or ER (Fig. 3C, Additional file 5:

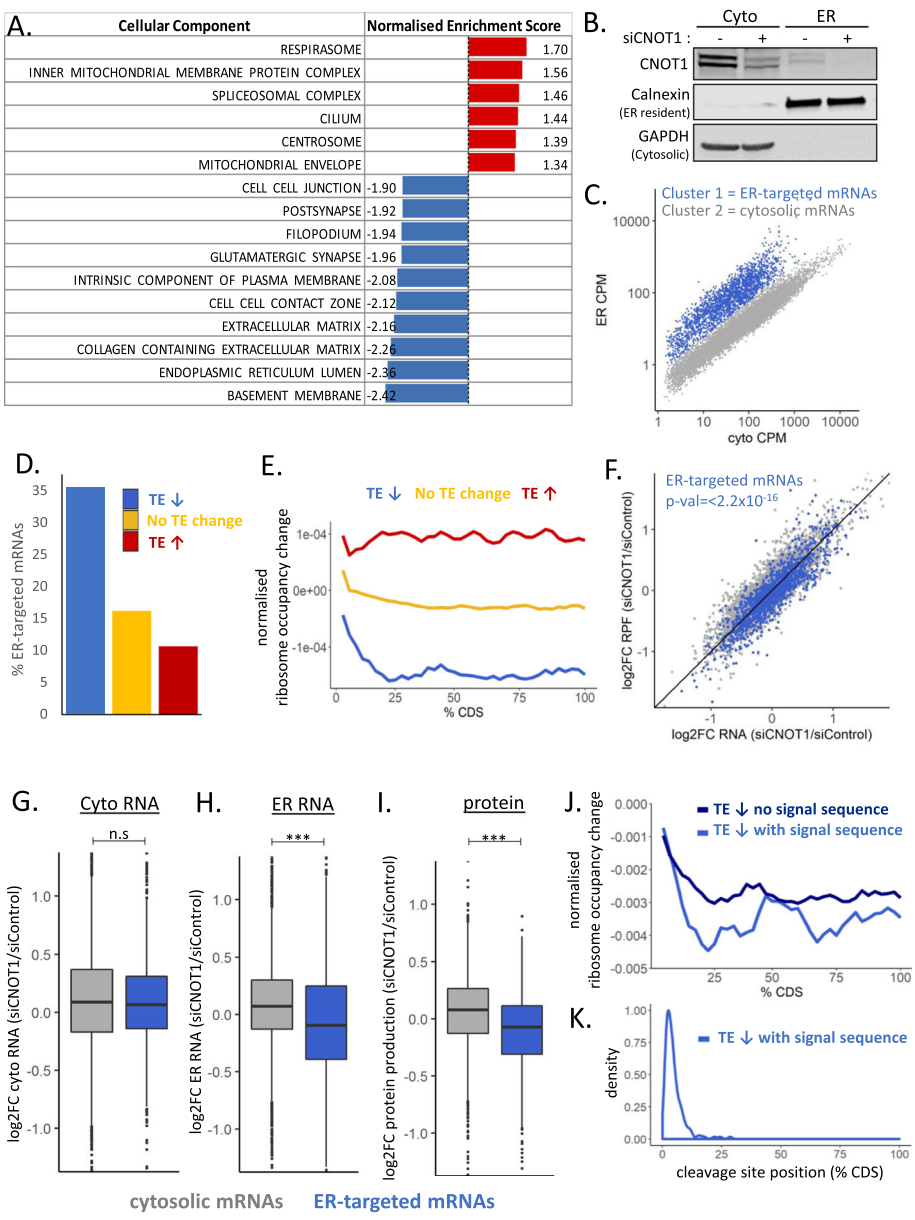

Fig. 3 ER-targeted mRNAs are translationally downregulated following CNOT1 depletion. **A** All mRNAs were ordered by the log2FC TE (siCNOT1/siControl) and gene set enrichment analysis conducted on the ranked list using the fgsea R package for cellular components. **B** Western blot confirming lysate fractionation into ER and cytosol with and without the depletion of CNOT1. **C** k-means clustering of mRNAs based on their abundance (CPM) in the ER and cytosolic fractions defines two groups of mRNAs based on their predominant localization. **D** mRNAs with decreased TE when CNOT1 is depleted (identified in Fig. 2C) are enriched for targeting to the ER in control conditions. **E** Median change in ribosome occupancy (normalized for mRNA abundance) assessed across the CDS for the groups of mRNAs identified in Fig. 2C. **F** ER-targeted mRNAs globally decrease translationally efficiency following CNOT1 depletion. **G** log2FC RNA in the cytosolic fraction between CNOT1 depleted and control conditions. **H** log2FC RNA in the ER fraction between CNOT1 depleted and control conditions shows a reduction in mRNAs that are targeted to the ER in control conditions localizing to the ER after CNOT1 depletion. **I** Displayed is the protein production change (siCNOT1/siControl) for mRNAs predominantly localized to the cytosol or the ER. For (**F–I**), significance was determined using the Kruskal-Wallis test. **J** Median change in ribosome occupancy (normalized for mRNA abundance) assessed across the CDS for the mRNAs with decreased TE after CNOT1 depletion separated into two groups based on the predicted presence of a signal sequence (determined using SignalP [91]). 157/899 mRNAs were predicted to contain a signal sequence. **K** Predicted location of the signal peptidase cleavage site in the group of mRNAs with a predicted signal sequence (determined using SignalP [91])

Table S4); using these groups shows a greater proportion of mRNAs translationally downregulated following CNOT1 depletion are indeed ER-targeted mRNAs in HEK293 cells (Fig. 3D) and the proteins encoded are localized at the ER and plasma membrane (Additional File 1: Fig.S7CD, data from U2OS cells [87]).

In contrast, mRNAs encoding proteins associated with the mitochondria, splicing, or the centrosome are translationally upregulated following CNOT1 depletion (Fig. 3A, Additional File 1: Fig. S7A). Increased TE is also associated with proteins involved in tRNA processing and modification as well as proteins having molecular functions involved in DNA binding and repression of transcription (Additional File 1: Fig.S7AB). Overall, this analysis suggests a role for the Ccr4-Not complex in the translational regulation of functionally distinct and spatially localized groups of mRNAs.

Decreased ribosome occupancy after CNOT1 depletion occurs downstream of signal sequences

Next, we examined the change in ribosome occupancy across the CDS. This showed for mRNAs with increased translational efficiency the increased ribosome occupancy is evenly distributed across the CDS (Fig. 3E). However, for translationally downregulated mRNAs, ribosome occupancy ramps down sharply from the start codon throughout the first ~ 10% of the CDS, followed by a large and even reduction across the final 75% of the CDS (Fig. 3E). This suggests these mRNAs require the presence of the Ccr4-Not complex for their efficient translation in the first section of their CDS in control conditions. For example, this may be the result of the presence of regulatory sequences in this region that control mRNA localization, such as the signal sequence recognized by the signal recognition particle (SRP), which would conform with our observation about the high abundance of ER-targeted mRNAs in this group (Fig. 3D). In addition, we see a highly significant global reduction in the translational efficiency of ER-target mRNAs following CNOT1 depletion (Fig. 3F), suggesting the Ccr4-Not complex specifically plays a role in the regulation of mRNAs that localize to the ER to be translated.

To investigate this further, we fractionated cells into the ER and cytosol with and without CNOT1 depletion (Fig. 3B) and sequenced the RNA from each fraction. Using the classification of mRNAs predominantly localized in the ER or cytosol in control conditions (Fig. 3C, Additional file 5: Table S4), we were able to assess how these mRNAs change localization after CNOT1 knockdown. This clearly shows that ER-targeted mRNAs have reduced levels specifically in the ER after CNOT1 knockdown (Fig. 3G,H).

To confirm the impact of the altered mRNA localization and translational efficiency of ER-targeted mRNAs on protein output, pulsed SILAC (stable isotope labelling by amino acids in culture [88]) was conducted following CNOT1 depletion (Additional File 1: Fig. S8A). A protein was only included in the analysis if it was detected in both the forward and reverse labelling technical replicates (Additional File 1: Fig. S8) and in at least two of the three biological repeats, this resulted in a group of 3495 proteins (Additional File 1: Fig. S8C, Additional file 6: Table S5). The pulsed SILAC confirms that the reduced TE of ER-target mRNAs is reflected in reduced protein synthesis (Fig. 3I).

Ribosome pausing can occur at the signal sequence [89] and if the mRNA is not correctly translocated to the ER for the continuation of its translation, this would result in

lower ribosome occupation of the latter part of the CDS—as we observe. A very recent publication observed disome populations at these signal sequences [90], and our data suggests the involvement of the Ccr4-Not complex in the regulation of these pause sites. To investigate this in more detail, SignalP [91] was used to select mRNAs with predicted signal sequences. Separation of the positional data by the presence or absence of predicted signal sequence shows sharper decline in ribosome occupancy for mRNAs with a predicted signal sequence (Fig. 3J). The SRP cleavage site, on average, is positioned at around 4.75% of the length of the CDS (Fig. 3K). This position coincides with the sharp decline in ribosome occupancy in the absence of CNOT1. This might suggest that the Ccr4-Not complex accelerates the progression of the ribosome through this site by either facilitating localization of the mRNA or the efficiency of cleavage. Thus, in the absence of the complex, ribosome occupancy downstream of this position is significantly diminished because the ribosomes cannot progress.

The impact of codons on Ccr4-Not complex mediated regulation of translational efficiency

Having observed that an increase in mRNA half-life after CNOT1 depletion positively correlates with the frequency of G/C-ending codons (Fig. 1F), the correlation of codon frequencies with the log2FC TE was next examined. This showed it is A/U-ending codons that positively correlated with an increase in TE after CNOT1 knockdown (Additional File 1: Fig. S9A). However, of note is the extent of these correlations which is not as strong as observed for mRNA half-life (Fig. 1F). Nevertheless, there is a strong distinction in the direction of the correlation based on the 3rd nt of the codon as indicated in magenta/cyan (Additional File 1: Fig S9A). To confirm the influence of this factor, the luciferase reporter system was utilized. The Renilla luciferase CDS is naturally rich in A/U-ending codons (74.5%); hence, the three G/C-ending codons (AUC, GUC & ACC) most negatively correlated with the TE change were substituted into the Renilla sequence at the corresponding synonymous codon positions. The translational efficiency was then determined using the luciferase activity / luciferase RNA level determined by qPCR with firefly luciferase used as a transfection control. This reporter clearly demonstrates that conversion of A/U-ending codons in the Renilla CDS to synonymous G/C-ending codons leads to a reduction in the extent of TE change after CNOT1 knockdown (Additional File 1: Fig. S9B). This TE change is a consequence of both altered luciferase activity and RNA level.

mRNAs with AU-rich CDSes and 3′UTRs have been shown to be enriched in p-bodies (sites of translational repression and mRNA storage) [92], and CNOT1 depletion prevents p-body formation [19]. We are able to clearly show, using the previously published HEK293 p-body transcriptome [93], that mRNAs translationally upregulated after CNOT1 knockdown are most enriched in p-bodies in control conditions (Additional File 1: Fig. S9C). The exact nature of p-bodies is not fully understood; they contain components of the deadenylation and decapping machinery [19, 94–99] and the role of deadenylation in their formation is debated [57, 92, 93, 100–104]. Our finding suggests that these specific mRNAs might undergo targeted translational repression by the Ccr4-Not complex followed by subsequent shuttling to p-bodies for storage.

How regulation of mRNA translation and/or stability by the Ccr4-Not complex impacts protein output

As we had determined that there is a global upregulation of both mRNA stability and translation following depletion of CNOT1, we next sought to understand the role of the Ccr4-Not complex in translation both alongside and independent of its role regulating mRNA stability. To dissect how the Ccr4-Not complex regulates mRNA translation compared to its control of stability, mRNAs were grouped based on the change in their translational efficiency (as assessed by ribosome profiling) and change in mRNA half-life (determined by triptolide inhibition) following CNOT1 depletion (Fig. 4A). This generates six groups of mRNAs classified first by whether there is decreased TE, no TE change, or increased TE (blue, yellow, and red, respectively, as in Fig. 2C), and second by a small change in mRNA half-life or a large increase in mRNA half-life (dark, light, respectively) when CNOT1 is depleted (Fig. 4A; Additional File 1: Fig. S10A).

Next the aim was to investigate how the observed translation and stability changes impact protein output by use of the pulsed SILAC data (Additional File 1: Fig. S8). The Ccr4-Not complex has a global role in the regulation of both mRNA stability and translation, and this is the first time the influence of this complex on protein output has been assessed. Analysis of protein-level changes in the differentially regulated groups of mRNAs (Fig. 4A). This shows that increased stability after CNOT1 knockdown results in increased protein synthesis compared to mRNAs with a minimal change in stability (light v dark colors, Fig. 4B). In addition, increased TE after CNOT1 knockdown is associated with increased protein synthesis (red v yellow, Fig. 4B) and decreased TE associated with decreased protein synthesis in comparison to mRNAs with a similar mRNA stability change but no change in TE (blue v yellow, Fig. 4B).

CDS composition differentiates how the Ccr4-Not complex regulates of mRNA translation vs stability

The Ccr4-Not complex has been shown to have roles in the regulation of both mRNA stability and translation [13–17, 19, 105]. To identify mRNA features that specifically influence how the complex regulates translation as opposed to stability, the importance of these variables in determining the mRNA group assignment (classification as in Fig. 4A) was evaluated using gradient boosting [71]. The feature analysis again points toward the CDS as a major driver for differential regulation of mRNA fate mediated via the Ccr4-Not complex, with the four most influential features pertaining to the CDS (Fig. 4C). Closer analysis of the top influential features shows it is shorter mRNAs that are most highly upregulated in terms of stability (Fig. 4D). The CDS GC content strongly distinguishes mRNAs with a large increase in half-life following CNOT1 depletion, from those with a lesser increase in half-life (Fig. 4E). Additionally, the AG content of the CDS distinguishes the translational changes between the groups of mRNAs with small increase in half-life (blue/yellow/red, Fig. 4F). mRNAs with increased translation are more AG-rich in the CDS than mRNAs with decreased translation (Fig. 4F).

In terms of 3′UTR features, the 3′UTR A content and length were the most influential for group classification (Fig. 4C). mRNAs with shorter 3′UTRs have increased TE with CNOT1 knockdown and mRNAs with decreased TE have longer 3′UTRs, with no influence of stability (Additional File 1: Fig. S10B). This suggests the translationally

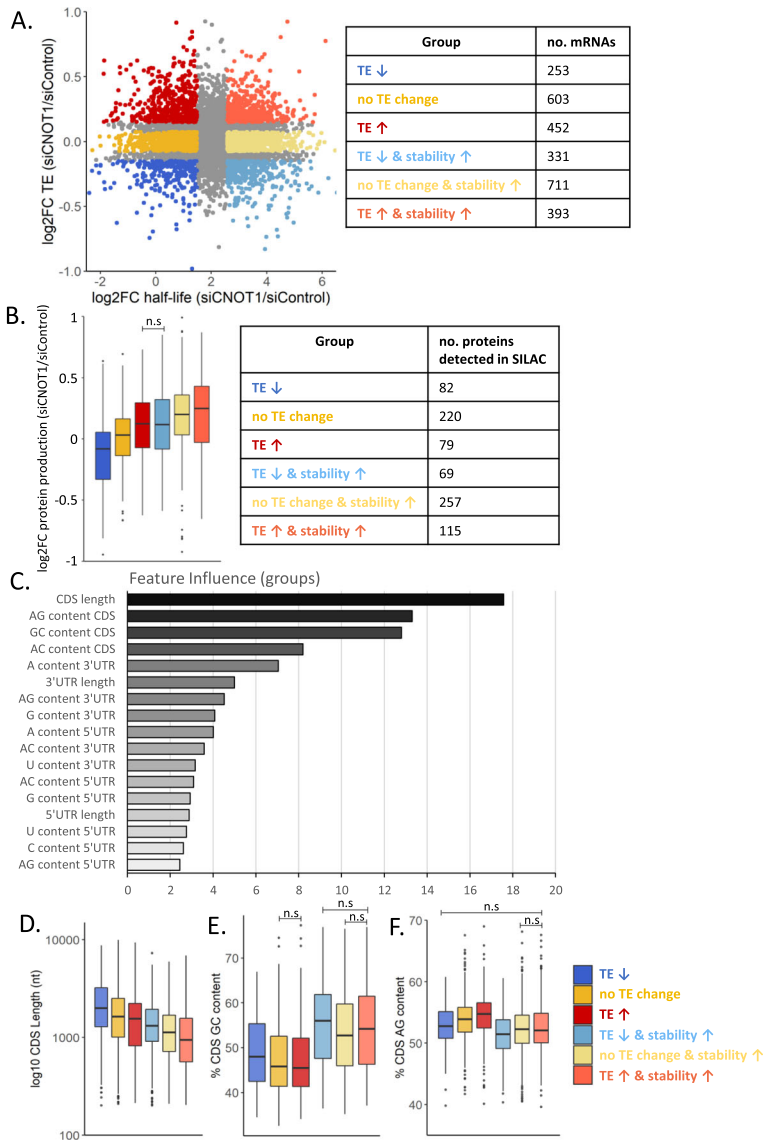

Fig. 4 mRNA features that distinguish the role of the Ccr4-Not complex in the regulation of mRNA translation v stability. **A** Data shows the log2FC in mRNA half-life after CNOT1 depletion (*x*-axis) compared to the log2FC translational efficiency (*y*-axis). mRNAs are first classified based on their mRNA stability change—a low log2FC mRNA half-life (dark colors) or a high log2FC mRNA half-life (light colors) and second by their TE change—increased TE (red), no TE change (yellow), or decreased TE (blue). **B** Pulsed SILAC data for three biological repeats conducted with forward and reverse labelling (Additional File 1: Fig. S8A-C). Displayed is the protein production change (siCNOT1/siControl) for the proteins that were detected in at least two biological repeats for the groups of mRNAs classified in (**A**). Non-significant comparisons are indicated, and all statistical comparisons are shown in Additional File 9: Fig. S1A. **C** The influence of mRNA sequence features on the classification of mRNAs into groups based how the Ccr4-Not complex differentially regulates their stability and/or translation (Fig. 4A) was determined by gradient boosting. **D–F** The presence of the top three features identified in (**D**) in the differentially regulated groups of mRNAs. **D** CDS length, **E** CDS G/C nucleotide content, and **F** CDS A/G nucleotide content. For clarity, non-significant comparisons are indicated, and all statistical comparisons are shown in Additional File 9: Fig. S1BCD

downregulated mRNAs may be more highly regulated as longer 3′UTRs means increased potential for the presence of regulatory sequences. Also, mRNAs with increased TE have a higher 3′UTR A content compared to the mRNAs with decreased TE that have a comparable half-life change (Additional File 1: Fig. S10C).

Overall, this analysis highlights a significant role for the CDS in coordinating Ccr4-Not complex function and further dissects the role of the complex in the regulation of translation compared to its roles in mRNA stability.

Nuclear proteins enriched for disorder-promoting AAs are translationally upregulated

We have shown that the frequency of G/C-ending codons is associated with mRNA destabilization by the Ccr4-Not complex (Fig. 1F), and feature analysis highlights the CDS composition as a distinguishing factor between differentially regulated groups of mRNAs (Fig. 4C–F). Analysis of average synonymous usage of codons for each of the groups of mRNAs revealed a strong distinction in the use of synonymous codons between mRNAs with a small and large increase in stability (Fig. 5A), in agreement with the earlier correlation data based on codon frequency (Fig. 1F). However, there are no additional major differences in synonymous codon usage preferences when dissecting this further to the level of altered translation (Fig. 5A). This suggests the synonymous codon usage is involved in how the Ccr4-Not complex regulates mRNA stability but is not a major determinant of its independent role in translation. Further investigation of how codon frequencies ultimately impact protein synthesis demonstrates that although the 3rd nucleotide preference of codons contributes to mRNA stability and translational efficiency regulated by the Ccr4-Not complex (Fig. 1F & Additional File 1: Fig. S9A), their frequency does not strongly correlate with protein production changes after CNOT1 depletion (Additional File 1: Fig.S9D).

We therefore examined the amino acid frequency in the differentially regulated groups of mRNAs. This shows, in addition to the synonymous codon usage, there is also a bias in the amino acid composition of these mRNAs (Fig. 5B). mRNAs with increased translation are enriched for polar/charged amino acids (AAs) and are depleted of non-polar amino acids (Fig. 5B). mRNAs with decreased translation show no preference for these same charged/polar amino acids (Fig. 5B). This suggests that it is a combination of codon and amino acid usage that influence how the Ccr4-Not complex regulates mRNA stability and translation and ultimately protein output.

Polar/charged AAs are often classified as disorder-promoting AAs in terms of their role in protein structure [106, 107]. Therefore, we examined the presence of these disorder-promoting AAs in the differentially regulated groups of mRNAs, which clearly showed they are enriched in the mRNAs with increase TE but minimal change in stability (Fig. 5C). AAs are important for protein function and can influence ribosome decoding speeds [78, 108, 109]. To understand the role of the disordered AAs in this group of mRNAs, we assessed the localization of the disordered AAs along the CDS. This showed the disordered AAs in the translationally upregulated group of mRNAs are enriched across the CDS and are particularly enriched at the 3′ end of the CDS compared to mRNAs with no effective TE change (Fig. 5D). Analysis of the protein class [110] of the mRNAs with increased TE showed an enrichment for transcription factors (TFs), specifically C2H2 zinc-finger TFs (Fig. 5E) and protein localization data confirms these translationally upregulated mRNAs encode proteins that are nuclear/chromatin localized (Additional File 1: Fig.S10D, data from [87]).

Unexpectedly, these zinc-finger protein mRNAs also have relatively short half-lives in control conditions, but do not show any change in mRNA stability with CNOT1

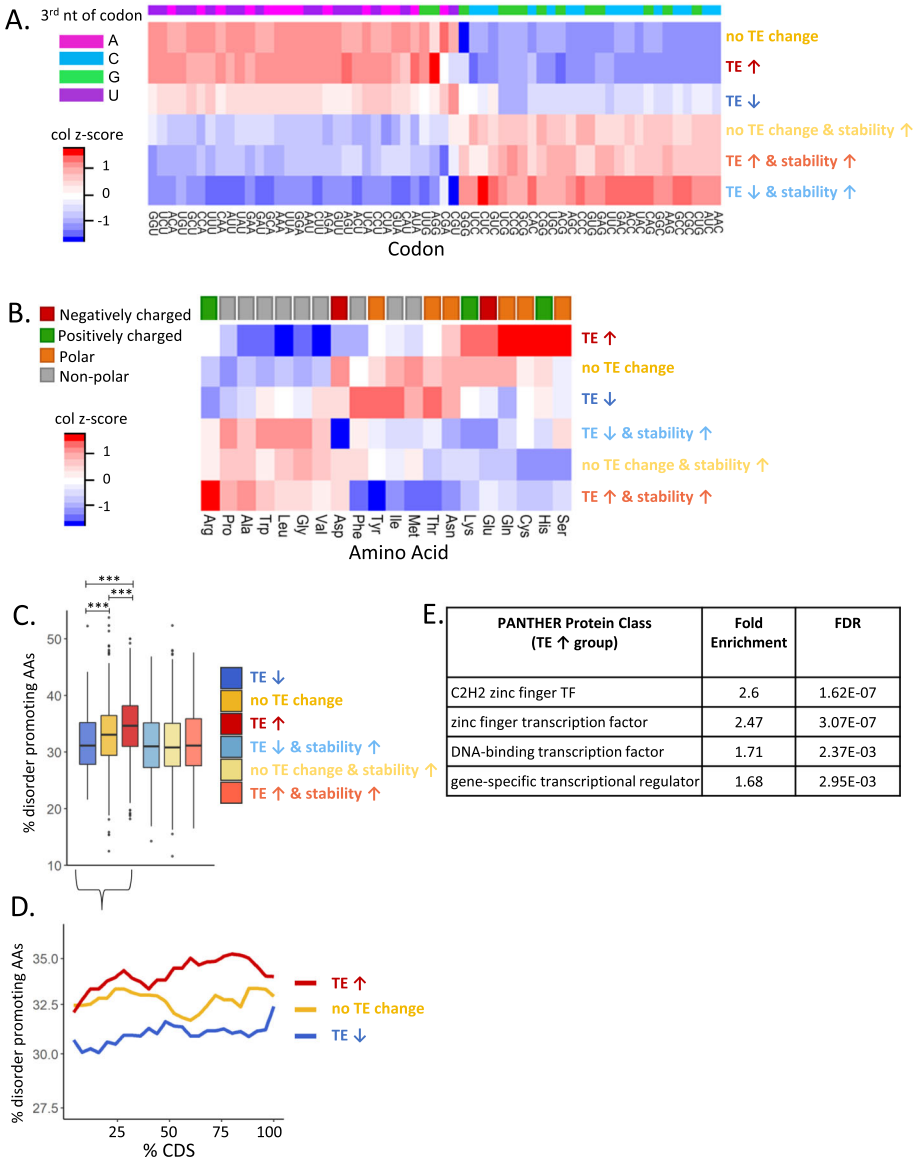

Fig. 5 Nuclear proteins enriched for disorder-promoting AAs are translationally upregulated. **A** Heatmap represents the synonymous codon usage of each codon that encodes a given amino acid and a column *z*-score has been applied to compare the codon preference between the groups of mRNAs. The colored bar at the top indicates the nucleotide present at the third position in the codon. **B** Heatmap shows the average frequency of each amino acid per mRNA and a column *z*-score has been applied. The colored bar at the top classifies the amino acids by their side chain type. **C** The percentage of amino acids encoded by the mRNAs that promote disorder in protein structure [106, 107]. Key significant comparisons are shown, and all statistical comparisons are presented in Additional File 9: Fig. S2A. **D** The localization of disorder-promoting amino acids across the CDS for the groups of mRNAs with minimal changes in mRNA stability. **E** Protein class enrichment analysis (using PANTHER [110]) shows that the mRNAs with increased TE but minimal increase in stability are enriched for transcription factors, specifically C2H2 zinc-finger proteins

depletion (Additional File 1: Fig. S10E). This is interesting because the mRNA turnover of this group of mRNAs appears completely independent of the Ccr4-Not complex, suggesting they are regulated by a distinct decay pathway and the Ccr4-Not complex is only involved in their translational regulation, perhaps linked to their specialized role in transcriptional control.

Ribosome pause sites regulated by the Ccr4-Not complex

The number of ribosomes on the mRNA at a point in time has often been used as an indicator of protein output—the more ribosomes on the mRNA the more translated the mRNA and hence the more protein produced. However, this is not always the case, both elongation and initiation rates dictate the overall ribosome occupancy observed at a single point in time. For example, decreased ribosome occupancy could be an indicator of removal of an elongation block resulting in increased elongation speed and therefore fewer ribosomes on the mRNA. Conversely, increased ribosome occupancy could be a result of either resolving a block at initiation of translation or decreased elongation speed which would result in slower run-off of ribosomes.

In yeast, it has been suggested that the Ccr4-Not complex is linked to ribosome pausing [12, 28]. Our ribosome profiling data with and without depletion of CNOT1 in HEK293 cells was utilized to examine this further in human cells. First, a pause site in each condition was defined as a position with a RPF peak height ten times greater than the average RPF peak on the mRNA. Second, these pause sites were then classified as either "sustained" meaning they are present but unaltered with CNOT1 knockdown; "resolved" in that the reduction in RPF peak height is ten times greater than the average delta decrease across the mRNA or "induced" in that the increase in RPF peak height is ten times greater than the average delta increase (Fig. 6A, Additional file 7: Table S6). Figure 6 B, C, and D show ribosome P-site occupancy for example mRNAs after normalization for mRNA abundance in control and CNOT1 knockdown conditions that contain the distinct pause site types (ribosome P- site shown and determined by read offset of 12 nt: Additional File 1: Fig. S11AB). It is possible for a specific mRNA to have pause sites meeting more than one of these criteria, Fig. 6A indicates the number of mRNAs containing combinations of these pause types, and the mRNAs distinctly with one type are used in downstream analysis to characterize these pause site types in more detail.

It has been proposed that the Ccr4-Not complex can sense paused ribosomes and trigger mRNA decay [28], and examination of the change in mRNA half-life with CNOT1 knockdown of the distinct pause type groups shows mRNAs with sustained and induced pauses undergo greater stabilization following CNOT1 depletion (Fig. 6E). This would fit with a model whereby the Ccr4-Not complex is involved in the sensing of stalled ribosomes and their resolution via decay mechanisms in that in the absence of CNOT1 the pauses are sustained or become pronounced.

In contrast, the mRNAs with pauses resolved by CNOT1 knockdown do not show an increase in mRNA half-life. To assess whether these are genuine sites of stalled ribosomes, the unique combination of pulsed SILAC and ribosome profiling data was used. We observe that the ratio between protein production and ribosome occupancy increases on mRNAs with resolved pause sites after CNOT1 depletion (Fig. 6F). This demonstrates that CNOT1 knockdown resolves ribosome pauses on these messages leading to altered translation and protein synthesis.

Next, we examined whether there are specific sequence motifs associated with these Ccr4-Not complex regulated pause sites. Figure 6 G, H, and I show the amino acid sequence motif at the E, P, and A-site and the 3 codons up- and downstream for each of the pause site types (created using Seq2Logo [111]). This shows a strong enrichment for charged amino acids, particularly glutamate, being encoded at the A-site position of

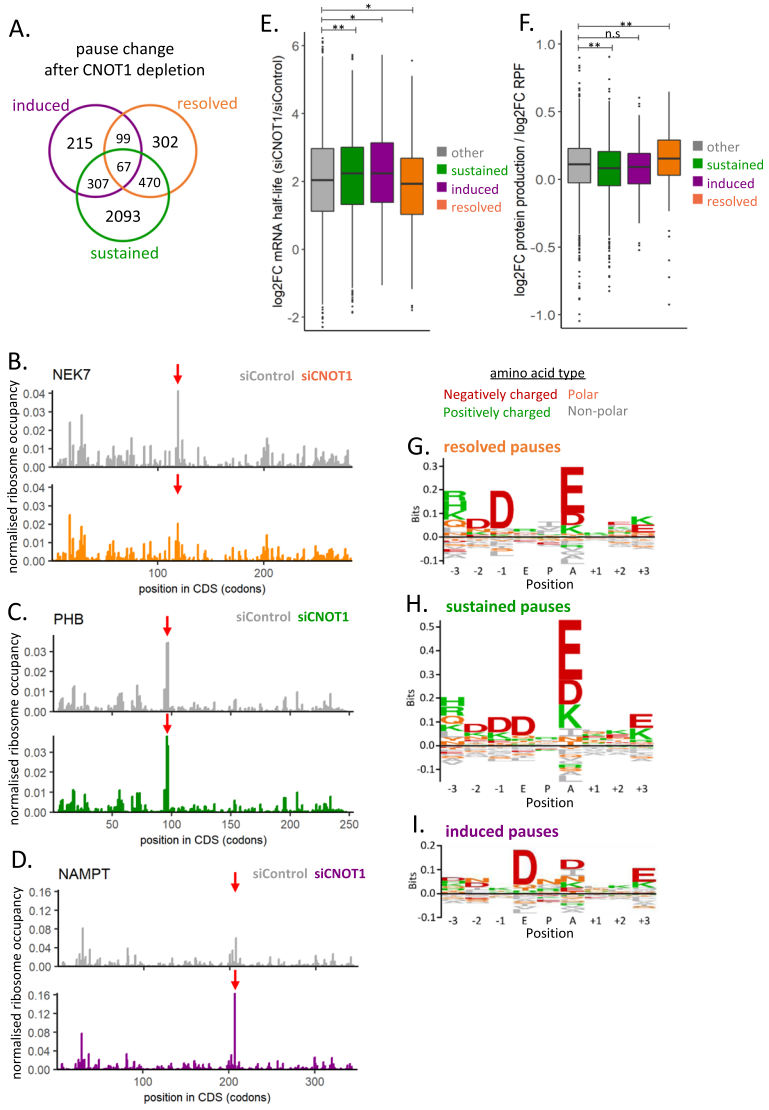

Fig. 6 Ribosome pause sites regulated by the Ccr4-Not complex. **A** Venn diagram indicates the number of mRNAs that contain pause sites sustained, induced, or resolved following the depletion of CNOT1. **B–D** Examples of individual mRNAs with different Ccr4-Not regulated ribosome pause types. **B** Pause resolved in the absence of CNOT1. **C** Paused sustained in the presence and absence of CNOT1. **D** Paused induced by CNOT1 knockdown. Plots show RPF coverage normalized for mRNA abundance (TPM). **E** The change in mRNA half-life after CNOT1 knockdown for the groups of mRNAs with different pause types identified in (**A**). **F** mRNAs with resolved pause sites in the absence of CNOT1 shown an increase in protein production relative to the ribosome occupancy on the mRNA when CNOT1 is depleted. **G–I** Amino acid sequence motifs at the E, P, A sites of paused ribosomes and three codons upstream and downstream generated using Seq2Logo [111], shown for resolved pauses (**G**), sustained pauses (**H**), and induced paused (**I**)

resolved and sustained pauses (Fig. 6G, H). This suggests this is a specific motif for ribosome pausing in control conditions, but there may be additional factors that determine precisely how the Ccr4-Not complex acts upon the pause site. A sequence motif at induced pause sites is not so pronounced but has an enrichment for aspartate at the ribosome E-site (Fig. 6I).

Previously, ribosome pausing on two specific proteasome component mRNAs in yeast has been shown to be regulated by Not1 to facilitate co-translational assembly [12].

Although there is still more to be elucidated about the precise mechanisms at play, this study now provides evidence for the role of the Ccr4-Not complex in the regulation of ribosome pausing in human cells and this regulation appears to be more widespread.

Discussion

Numerous mechanisms for mRNA specific recruitment of Ccr4-Not complex exist, whereby sequence motifs, predominantly in the 3′UTR, are recognized by sequence specific RNA-binding proteins or microRNAs, resulting in the delivery of the Ccr4-Not complex to the mRNA [61, 82, 112–115]. Importantly the Ccr4-Not complex has been shown to be able to exert both translational inhibition and mRNA destabilization and that these effects can occur separately [39, 41].

The CNOT1 subunit of the Ccr4-Not complex functions as a scaffold protein bringing into proximity the core subunits, and regulatory proteins to coordinate the varied roles of the complex [5, 116, 117]. CNOT1 also interacts with proteins such as TNRC6 that recruit the Ccr4-Not complex to the mRNA during miRNA-mediated repression [80, 112]. Here we have depleted CNOT1 to examine the global effects upon mRNA stability (Fig. 1, Additional File 1: Fig. S1,2), the translational status of the mRNAs (Fig. 2, Additional File 1: Fig. S4,5), and protein production (Fig. 4B, Additional File 1: Fig. S8). This is the first such comprehensive investigation of this multifunctional protein complex and provides a benchmark dataset for translational studies. We demonstrate for the first time in human cells how the Ccr4-Not complex differentially regulates cohorts of mRNAs and how translational repression is distinct from how the complex regulates mRNA deadenylation and stability.

Codon usage, and more recently amino acid usage, has been associated with differences in mRNA stability in control conditions in multiple organisms [51, 52, 77, 79, 118–120]. An example is reporter studies in yeast that have shown that substitution of optimal codons with synonymous non-optimal (generally A/U-ending) ones reduces mRNA stability [52]. Recent studies in human cells have also found A/U-ending codons to be destabilizing [79, 120], whereas another study has found G/C-ending codons to be destabilizing [92]. It is of note that this differential regulation may change with cellular context as it has been demonstrated that mRNAs preferentially involved in proliferation (enriched for A/U-ending codons) and differentiation (enriched for G/C-ending codons) have distinct codon usage and the tRNA pool available is altered to reflect this [75, 76, 121]. Thus, the inconsistency in whether it is the A/U-ending or G/C-ending synonymous codons that are classified as destabilizing in the literature could be explained by conditional differences.

Moreover, there is minimal understanding of the proteins involved in coordinating the response to codon usage. Previous research in yeast and zebrafish has implicated subunits of the Ccr4-Not complex in codon-mediated regulation of mRNA stability [16, 28, 72]. We show that knockdown of CNOT1 preferentially stabilizes mRNAs enriched in G/C-ending codons (Fig. 1D, F, Fig. 5A) and thus show the central role of the Ccr4-Not complex in the link between mRNA stability and codon usage in human cells. Studies of the translatome and mRNA half-life are not often complemented with protein-level data. Unexpectedly, we show that while large changes in mRNA stability attributable to codon composition of the CDS are observed (Figs. 1F and 5A), these correlations are not apparent in the pulsed SILAC data (Additional File 1: Fig S9D).

Gene ontology analysis highlighted that increased mRNA half-life after CNOT1 knockdown is associated with an enrichment for biological processes relating to cardiac septum and muscle organ development (Additional File 1: Fig. S3A), which is particularly interesting given that recent publications demonstrate the importance of CNOT1 for cardiac development [68] and neurodevelopment [122]. Decreased translational efficiency in the absence of CNOT1 is observed for mRNAs encoding proteins involved in extracellular structure organization that preferentially localize to the ER and plasma membrane (Fig. 3, Additional File 1: Fig. S7). We also find that the reduced ribosome occupancy among this group of mRNAs following CNOT1 depletion occurs downstream of the signal sequence cleavage site (Fig. 3J, K) and reduced localization of mRNAs to the ER after CNOT1 depletion (Fig. 3H). An intriguing hypothesis would be that one of the translational control mechanisms mediated by the Ccr4-Not complex is coordination of subcellular localization of mRNA.

In addition, our data shows a role for the Ccr4-Not complex in the translational repression of mRNAs that are localized to p-bodies (Additional File 1: Fig. S9C). It will be interesting to investigate in the future whether this is due to an indirect role of CNOT1 in p-body formation [19] or if the Ccr4-Not complex is also involved in mediating repression that occurs within these granules. The mRNAs translationally upregulated following CNOT1 depletion encode transcription factors/nuclear proteins (Fig. 5E, Additional File 1: Fig S10D), in agreement with p-body studies [92, 93]. They are also enriched for amino acids associated with disordered regions in the proteins (Fig. 5C), intrinsically disordered regions have been suggested to be the regions of transcription factors that interact with the promoter region [123, 124]. Also, the tertiary structure of zinc-finger domains has been shown to be able to act as a nuclear localization sequence [125, 126], so perhaps the distinct amino acid composition of this group of mRNAs pertains to the localization and protein function.

Finally, we identify groups of mRNAs on which ribosome pausing occurs in a CNOT1-dependent manner (Fig. 6A). These pauses impact how the Ccr4-Not complex regulates mRNA half-life (Fig. 6E) and protein synthesis (Fig. 6F). There is an enrichment for charged amino acids at the A-site of paused ribosomes in the presence of CNOT1 (Fig. 6G, H). Whether there are additional proteins and/or sequence motifs that determine precisely how the Ccr4-Not complex regulates the fate of mRNAs with paused ribosomes could be investigated in the future.

Conclusions

Here we have demonstrated that the CDS composition of an mRNA is important for the regulation of its fate by the Ccr4-Not complex in terms of codon usage and CDS length. In this cellular context, G/C-ending codons mediate the destabilization of an mRNA by the Ccr4-Not complex. We also discover a novel role for the Ccr4-Not complex in the regulation of the localization of mRNAs to the ER for their translation. Moreover, mRNAs encoding proteins that localize to the nucleus are regulated at the level of translation by the Ccr4-Not complex and are sequestered in p-bodies in control conditions. Overall, we show that the Ccr4-Not complex is a control hub that governs multiple mechanisms to precisely regulate the fate of each mRNA.

Experimental methods

Cell culture

HEK293 cells were cultured in Dulbecco's modified Eagle's medium (DMEM) supplemented with 1% L-glut and 10% FBS. The HEK293 cell line was not validated and cells were routinely tested for mycoplasma.

siRNA treatment

Control siRNA (#3 Dharmacon) or CNOT1 siRNA (Ambion no. S22844) was transfected using DharmaFECT 1 (2:1 ratio of siRNA to DharmaFECT 1) to a final concentration of 30 nM and cells harvested after 48 h. Due to CNOT1 siRNA treatment causing slowed cell growth, cells for CNOT1 siRNA treatment were plated at 10% increased density to obtain the same cell numbers as the control samples at the time of harvesting. For experiments in Additional File 1: Fig. S2DEF & Fig. S9B, an additional siRNA pool targeting CNOT1 was used (Horizon Discovery 015369-01).

Antibodies

For western blot, the antibodies used were as follows: CNOT1 (ATLAS HPA Rabbit 046577, 1:500), vinculin (abcam mouse ab18058, 1in 10,000), GAPDH (CST 5174, 1:1000), Calnexin (CST 2679, 1:1000), rabbit secondary antibody (LI-COR Biosciences 926-32213, 1:10,000), mouse secondary antibody (LI-COR Biosciences 926-68072, 1:10,000). Uncropped western blots are presented in Additional File 3.

Ribosome profiling

Ribosome profiling was conducted as previously described in Wilczynska et al.. In parallel to these control experiments, ribosome profiling was conducted for samples transfected with CNOT1-targeting siRNA for 48 h. Three biological replicates were conducted.

RT-qPCR from gradient fractions

For validation experiments, media was changed on a 15-cm plate of HEK293 cells 1.5 h prior to harvesting. Cells were then scraped in ice-cold PBS, spun down, and resuspended in lysis buffer containing cycloheximide. Then, 300 μl lysate was loaded on to a 10–50% sucrose gradient then spun at 38,000 rpm for 2 h at 4 °C. Gradient fractions were collected into 3 ml 7 M GuHCl, 8 μl glycogen, and 4 ml ethanol added and then precipitated for > 24 h at − 20 °C. The collected gradient fractions were pelleted at 4000 rpm for 1 h at 4 °C. The supernatant was removed, and the pellets resuspended in 400 μl RNase-free water. The samples were then transferred to 1.5-ml Eppendorfs, 2 μl glycogen, 40 μl 3 M NaOAc pH 5.2, and 1 ml 100% ethanol added. These were precipitated overnight at − 20 °C. Samples were then pelleted at 13,000 rpm 4 °C for 40 min, washed with 500 μl 75% ethanol, air dried, and resuspended in 30 μl RNase-free water. To check the RNA integrity, equal volumes (3 μl) of each fraction along the gradient were ran on a 1% agarose gel.

RT-PCR was conducted on equal volumes (3 μl) of each fraction using SuperScript III (Invitrogen 18080085). qPCR was then conducted using SYBR Green master mix (Applied Biosystems 4385618) on an Applied BioSystems QuantStudio 5 machine. For

qPCR along the gradient fractions, the proportion of the mRNA present in fraction was plotted. All qPCR primers used are included in Additional file 8: Table S7.

Cell viability

Cells were grown in 12-well plates and treated with a range of triptolide concentrations. Then, 100 μl trypsin was added per well and 200 μl media added to quench this. Ten microliters of cells was then mixed with 10 μl tryphan blue, and cells negative and positive for tryphan blue were counted using a hemocytometer.

Transcriptional inhibition experiments

For the transcriptional inhibition experiments to determine mRNA half-lives, cells were plated in 12-well plates and transfected with control or CNOT1-targeting siRNA for 48 h. The medium was changed 1 h prior to treatment with 1 μM triptolide (abcam: ab120720). At a range of time points (0, 0.5, 1, 2, 4, 8, and 16 h) post-triptolide addition, cells were washed with PBS and lysed directly in 1 ml of Trizol for RNA samples or 150 μl 1.5× SDS sample buffer for protein samples. Three biological replicates were conducted. The RNA was extracted with Trizol and acid-phenol chloroform. Three micrograms of RNA was then poly(A) selected (Lexogen 039.100). Four nanograms of poly(A) selected RNA was used as input into the CORALL Total RNA-Seq library prep kit (Lexogen 096.96) with 11 PCR cycles used. For qPCR validations (Additional File 1: Fig S2DEF), 1 μM flavopiridol was used and 100 ng/μl oligodT used in the RT reaction.

Cytoplasmic/ER fractionation

Fractionation of cytoplasmic and ER material was performed by sequential detergent extraction, as previously reported (Reid, JBC, 2012). An isotonic buffer (20 mM Tris pH 7.4, 150 mM NaCl, 5 mM $MgCl_2$) was supplemented with 1 mM DTT, 1× cOmplete EDTA-free protease inhibitor (Roche). For sequential lysis, it was further supplemented with 0.015% digitonin (cytosolic buffer), or 0.004% digitonin (wash buffer), or 2% n-Dodecyl β-D-maltoside (ER buffer). Then, 80 U/ml of Ribolock RNase Inhibitor (Thermo Scientific) was added to each final buffer. Two thirds of each sample was processed for RNA extraction with Trizol LS, and 5× SDS sample buffer added to the remaining lysate for western blotting.

Prior to library preparation, ERCC spike-ins (Invitrogen) were added proportionally between the cytosolic and ER fraction in each condition. In total, 900 ng of RNA was rRNA depleted with the RiboCop rRNA Depletion Kit HMR V2 (Lexogen) and library preparation performed with the CORALL Total RNA-Seq Library Prep Kit (Lexogen 096.96). Sequencing was performed on a NextSeq 550 system (Illumina).

Pulsed SILAC (stable isotope labelling by amino acids in cell culture)

These experiments were conducted as described in Wilczynska et al. (repeat 1—forward and reverse—is the data used in Wilczynska et al.). In brief, HEK293 cells were cultured and siRNA treated for 30 h. This media was then replaced with DMEM that does not contain arginine or lysine (Life Technologies). For the medium-heavy isotope-containing medium, a supplement of [13C6] L-arginine (Arg-6) and [2H4] L-lysine

(Lys-4) was added (Cambridge Isotope Laboratories). For the heavy isotope-containing medium, [13C6][15 N4] L-arginine (Arg-10) and [13C6][15 N2] L-lysine (Lys-8) were added (Cambridge Isotope Laboratories). Both forward (heavy CNOT1 siRNA/medium-heavy control siRNA) and reverse (medium-heavy CNOT1 siRNA/heavy CNOT1 siRNA) replicates were conducted for each biological repeat. After 14 h, cells were lysed in SDS-free RIPA buffer, pooled in a 1:1 ratio, reduced with DTT and alkylated with iodoacetamide. The samples were then trypsin digested and fractionated using reverse phase chromatography. For the exact details of the analysis of the samples by mass spectrometry and the data analysis with MaxQuant software [127], see Wilczynska et al 2019. **A protein** was retained for downstream analysis if it was detected in the forward and reverse replicate for a given biological repeat, and if detected in at least two of the three biological repeats.

Luciferase reporter experiments

Twenty-four hours after siRNA transfection in 12-well plates, cells were transfected with 40 ng pRL and 160 ng pGL3 intron as a transfection control (Meijer NAR 2019) using 0.6 μl GeneJammer (Agilent). The Renilla construct (pRL) was either the original sequence or a sequence with all the AUU/GUU/ACU codons converted to their synonymous codons (AUC/GUC/ACC). After another 24 h, samples for detection of luciferase activity were washed twice with PBS and lysed in 1× passive lysis buffer, and 10 μl lysate used for luciferase detection using the Dual Luciferase Reporter Assay System (Promega). Samples for RNA were harvested in 1 ml Trizol. Relative luciferase activity was determined by the ratio between Renilla and Firefly luciferase and the relative luciferase RNA levels determined by qPCR. The translational efficiency of Renilla was then determined by luciferase activity / RNA level.

Data analysis methods

mRNA half-life experiment RNA sequencing data processing

Cutadapt [128] was used to remove adapters. cd-hit-dup [129] was used to deduplicate the reads based on the 12-nt-long UMIs. The remaining reads were aligned to the genome using STAR [130] and a gtf file filtered to contain the most abundant transcript per gene. To obtain the read counts featureCounts [131] was used with the gtf file filtered for the most abundant transcript per gene. The read counts were first normalized for the library size. As the libraries are prepared based on equal ng of material, the read counts are normalized back to the nanodrop concentrations of the RNA that was obtained from equal cell numbers. For each condition, the data was then normalized relative to the 0 h time point to allow for comparison between mRNAs and conditions.

Modelling mRNA decay rate

To be able to use the three replicates together in the decay modelling, for each replicate the values for each mRNA across the time points were normalized to the 0 h time point (set at 100). The simple model for mRNA decay is that it follows the exponential decay function: $y \sim y_0 e^{-kt}$. Where y_0 is the steady-state mRNA level, k is the decay constant and t is time. Outliers were first identified based on the methodology described in [132]. The nlrob function (R package: robustbase) was used to fit a robust nonlinear

model to the data with an adapted from of the NLS.expoDecay function (R package: aomisc) to provide start parameters for the model fit. To next identify possible outliers, the weighted residual was calculated: weighted residual = absolute (observed − expected)/expected. The maximum proportion of outliers was set to 20% to ensure natural biological variation was not mistaken for an outlier. The robust standard deviation of residuals (RSDR [132];) was then calculated by ranking the residuals in terms of absolute value and taking the value at the 68.27 percentile and multiplying this value by $N/(N - K)$, where N is the number of values and K is the number of parameters being modelled. The significance level for outlier removal is $\alpha_i = Q(N - (i - 1))/\mathrm{N}$, where N is the number of values in the data and i is the ith value in the ordered list of residuals. Q was set to 5% (0.05) and this means that there is a 5% chance of falsely discovering a significant outlier. The t-score in this case in then calculated by: t-score = residual$_i$/RSDR [132]. The pt function (R package: stats) is then used to obtain the two-tailed p value of the t-score. If this p value is less than α_i, then this value is a significant outlier.

Once significant outliers had been removed, the modelling was conducted in R using the nls function from the stats package. To ensure appropriate starting parameters were used in the modelling a self-starting function was used—NLS.expoDecay() part of the aomisc R package. The half-lives were then calculated from the decay rate using the equation: $t_{1/2} = \ln(2)/k$.

Assessment of feature influence

To assess which mRNA features contribute to differential regulation of mRNA fate by the Ccr4-Not complex, a supervised learning approach of gradient boosting (gbm R package) was used (Figs. 1D and 4C). Only one of highly correlated features ($r > 0.7$) were retained for the analysis (Additional File 1: Fig. S3B). For Fig. 1D, a Gaussian distribution was assumed and for Fig. 4C a multinomial distribution. The parameters used were as follows: n.trees = 200, interaction.depth = 6, shrinkage = 0.005, cv.folds = 10.

Ribosome profiling—small RNA alignment and counts

For the small RNA sequencing data (ribosome protected fragments: RPFs), Cutadapt [128] was used to remove the adapter sequence and the reads were deduplicated based on the 8-nt unique molecular indexes (UMIs—4 nt either end of the read) using cd-hit-dup [129]. Cutadapt [111] was then used to remove UMIs and to select read lengths 25 to 35 nt (the expected size range of the RPFs). The reads were first aligned to a fasta file of rRNA sequences, to remove contaminant rRNA fragments by alignment with bowtie [133]. The reads were then mapped with bowtie to the hg38 gencode version 28 [134]) protein coding transcriptome that had been filtered for the most abundant transcript per gene as determined from the control total RNA-seq data.

To get the number of RPFs per gene and the exact position of the RPFs along the mRNA, a python script from the RiboCount part of the RiboPlot package (https://pythonhosted.org/riboplot/) was adapted. This was first conducted for each read length to determine the frame, periodicity, and P-site offset for each read length. It was determined that read lengths 27 to 31 showed strong RPF characteristics, thus these read lengths were selected for downstream analysis. E, P, and A-site offset were determined to be 9 nt, 12 nt, and 15 nt from the read start respectively (see Additional File 1: Fig.

S11AB). For figures of ribosome position across individual mRNAs, the P-site position was used (Fig. 6B–D, Additional File 1: Fig.S6).

Ribosome profiling—total RNA alignment and counts

For the corresponding total mRNA samples, cutadapt [128] was used to remove adapter sequences, cd-hit-dup [129] to deduplicate based on the 8 nt UMI. The UMI was then removed with cutadapt, and the sequences aligned with STAR [130] to a gtf file filtered for the most abundant transcript per gene. Bam files were sorted and indexed using SAMtools [135]. Read counts were obtained using htseq-count [136].

DESeq2 differential expression analysis

DESeq2 [85, 86] was used for differential expression analysis of the RNA and RPFs following CNOT1 knockdown. As the RPFs and RNA are very different library types, something the DESeq2 package is not able to account for, the differential expression analysis was conducted independently for the two datasets. The data was pre-filtered to ensure at least three samples had a minimum of 10 read counts for any given mRNA. To ensure that lower abundance mRNAs or lowly translated mRNAs do not have an exaggerated fold change, the lfcShrink function with apeglm model of the DESeq2 package was used for effect size estimations [86]. Log2FC translational efficiency was calculated as log2FC RPF – log2FC RNA from the DESeq2 results (Additional File 3: Table S2). DESeq2 was also used in the same manner to determine the log2FC in RNA in cytosolic and ER fraction following CNOT1 depletion (Additional File 5: Table S4).

Differential ribosome occupancy across the CDS

For the total RNA data, transcripts per million (TPM) was calculated. For the RPFs, the read data was normalized for library size and for each read the nucleotide of the P-site start used (12 nt offset from read start). RPF counts at each position along the CDS of each mRNA were then normalized for the mRNA abundance using the TPM from the total RNA-seq. After this normalization to account for mRNA abundance changes, for each biological replicate a delta was conducted for the normalized RPF coverage along each mRNA between CNOT1 and control siRNA conditions. The delta for each mRNA was then averaged for the three biological replicates. For Fig. 3E, J, the delta in the distinct groups of mRNAs was binned into 40 windows across the CDS to account for the different CDS lengths of the mRNAs and the median change in ribosome occupancy in each window displayed.

Gene Set Enrichment Analysis

Normalized enrichment scores for biological process, cellular component, and molecular function gene sets were calculated using the fgsea R package. Significant enrichment was determined using an adjusted p value threshold of < 0.05. The full list of significant results is in Additional File 4: Table S3.

Synonymous codon usage

Synonymous codon usage is based on the fact that for many amino acids there are multiple codons that encode it. For each codon, the number present within a given CDS

were counted and then normalized for the total number of possible codons that can encode the same amino acid in that CDS. This was conducted for each mRNA, and then for the distinctly regulated groups of mRNAs, this was then averaged across the group. The heatmaps are column-scaled as the comparison being made is the preferential use of the codons between the different groups of mRNAs (Fig. 5A). The colored bar indicates the nucleotide at the third position of the codon.

Amino acid usage

For amino acid usage, the frequency of codons for each amino acid were counted per mRNA and normalized for the number of codons in the mRNA. The frequency for each amino acid was then averaged across the group of mRNAs (if the amino acid frequency for an mRNA was zero, it was excluded from the average). The heatmaps are column-scaled as the comparison being made is the use of the amino acid between the different groups of mRNAs (Fig. 5B). The colored bar indicates the type of amino acid side chains. For Fig. 5C, D, amino acids were classified as disorder-promoting (P|Q|E|S|K) as in [106].

Ribosome pause site determination

For analysis of paused elongating ribosomes, all RPFs apart from those located in the first 15 and last 5 codons of the CDS were used. A pause site in each condition was defined as a position with a RPF peak height ten times greater than the average RPF peak on the mRNA. The change in peak height between conditions was determined as a delta between RPFs that had been normalized for the mRNA abundance (TPM). Pause sites were then classified as either "sustained" if there was no change in peak height; "resolved" if RPF peak height decrease was ten times greater than the average delta decrease across the mRNA; or "induced" if the increase in RPF peak height was ten times greater than the average delta increase (Fig. 6A). The mRNAs distinctly with one type of pause site are used in downstream analysis and the exact pause positions are indicated in Additional File 7: Table S6.

Motif analysis

For the amino acid motifs generated in Fig. 6G–I, the Seq2Logo web app was used [111]. The settings used were P-Weighted Kullback-Leibler logo type, Hobohm1 clustering method, and 200 weight on prior.

k-means clustering

For clustering of mRNAs based on their half-lives (Fig. 1B) in the presence and absence of CNOT1, the half-life values were log transformed and the optimal number of clusters determined using within cluster sum of squares. The factoextra R package was used for k-means analysis and cluster visualization. For clustering of mRNAs into ER-targeted and cytosolic mRNAs in control conditions (Fig. 3C), the RNA-seq counts were first transformed into counts per million (CPM) and adjusted using the ERCC spike-in sequences to account for differences in absolute RNA levels between the cytosolic and ER fractions.

Statistics

The Kruskal-Wallis test was used for Fig. 3F–I. For all the figures requiring multiple comparisons, the Dunn test (FSA R package) was used to determine significance and Benjamini Hochberg method applied to correct for multiple hypothesis testing. For the groups of mRNAs distinctly regulated by the Ccr4-Not complex as identified in Fig. 4A, the full set of statistical comparisons between the data for each group are included in tables in Additional File 9 for clarity. *** indicates p.adj < 0.001, ** p.adj < 0.01 & * p.adj < 0.1. For Additional File 1: Fig S9B, a two-tailed paired *t*-test was used.

Supplementary Information

The online version contains supplementary material available at https://doi.org/10.1186/s13059-021-02494-w.

Additional file 1. Supplementary figures.
Additional file 2: Table S1. log2FC mRNA half-life.
Additional file 3: Table S2. log2FC RNA & log2FC RPF (DESeq2 data).
Additional file 4: Table S3. Gene Ontology fgsea results.
Additional file 5: Table S4. ER/cyto fractionation RNA-seq.
Additional file 6: Table S5. pulsed SILAC.
Additional file 7: Table S6. pause site types.
Additional file 8: Table S7. qPCR primer sequences.
Additional file 9. Statistics for Main Figures 4 and 5C and Additional file 1: S10 B/C.
Additional file 10. Uncropped Western blots.
Additional file 11. Review history.

Review history

The review history is available as Additional file 11.

Peer review information

Andrew Cosgrove was the primary editor of this article and managed its editorial process and peer review in collaboration with the rest of the editorial team.

Authors' contributions

SG, AW, and MB designed the experiments and wrote the manuscript. SG performed the ribosome profiling, transcriptional inhibition experiments, qPCR validations, and all bioinformatic analysis. CG conducted ER/cyto fractionation experiments. AW, KH, and SZ designed and conducted the pulsed SILAC experiments. All authors have approved the final manuscript.

Funding

This work was conducted in the MB lab and supported by Cancer Research UK core grant numbers A29252 & A31287, core funding from the Medical Research Council MC_UP_A600_1024, MRC Senior Fellowship to MB MC_EX_G0902052, BBSRC BB/N017005/1, and BBSRC BB/M001865/1. We would like to thank the Core Services and Advanced Technologies at the Cancer Research UK Beatson Institute (C596/A17196), with particular thanks to the Proteomics team.

Availability of data and materials

The datasets generated and/or analyzed during the current study are available in the GEO and ProteomeXchange repository. Transcriptional inhibition experiments RNA-seq data have been deposited under GSE158619 [137]. Ribosome profiling experiments (both small RNA and total RNA libraries) have been deposited under GSE158141 [138]. RNA-seq of mRNA in ER and cytosol fractions with and without depletion of CNOT1 is deposited under GSE183148 [139]. SILAC data is deposited under PXD015772 (repeat 1) [140] and PXD020305 (repeats 2 and 3) [141]. Code used for the analysis is available on github under a GNU General Public License v3.0 [142].

Declarations

Ethics approval and consent to participate

Not applicable.

Competing interests

The lab collaborates with Cancer Research UK's Therapeutic Discovery Laboratories on drug discovery against some of the targets mentioned in this paper.

Author details
[1]Cancer Research UK Beatson Institute, Garscube Estate, Switchback Road, Glasgow G61 1BD, UK. [2]MRC Toxicology Unit, Lancaster Road, Leicester LE1 9HN, UK. [3]Institute of Cancer Sciences, University of Glasgow, Glasgow, UK.

Received: 29 October 2020 Accepted: 10 September 2021
Published online: 06 October 2021

References

1. Albert TK, Lemaire M, van Berkum NL, Gentz R, Collart MA, Timmers HT. Isolation and characterization of human orthologs of yeast CCR4-NOT complex subunits. Nucleic Acids Res. 2000;28(3):809–17. https://doi.org/10.1093/nar/28.3.809.
2. Collart MA. The Ccr4-Not complex is a key regulator of eukaryotic gene expression. Wiley Interdiscip Rev : RNA. 2016;7:438–54 Blackwell Publishing Ltd.
3. Denis CL, Chen J. The CCR4-NOT complex plays diverse roles in mRNA metabolism. Prog Nucleic Acid Res Mol Biol. 2003;73:221–50. https://doi.org/10.1016/S0079-6603(03)01007-9.
4. Ukleja M, Cuellar J, Siwaszek A, Kasprzak JM, Czarnocki-Cieciura M, Bujnicki JM, et al. The architecture of the Schizosaccharomyces pombe CCR4-NOT complex. Nat Commun. 2016 Jan;25(1):7. https://doi.org/10.1038/ncomms10433.
5. Xu K, Bai Y, Zhang A, Zhang Q, Bartlam MG. Insights into the structure and architecture of the CCR4-NOT complex. Front Genet. 2014;5:137.
6. Liu HY, Badarinarayana V, Audino DC, Rappsilber J, Mann M, Denis CL. The NOT proteins are part of the CCR4 transcriptional complex and affect gene expression both positively and negatively. EMBO J. 1998;17(4):1096–106. https://doi.org/10.1093/emboj/17.4.1096.
7. Badarinarayana V, Chiang YC, Denis CL. Functional interaction of CCR4-NOT proteins with TATAA-binding protein (TBP) and its associated factors in yeast. Genetics. 2000;155(3):1045–54. https://doi.org/10.1093/genetics/155.3.1045.
8. Denis CL, Chiang Y-C, Cui Y, Chen J. Genetic evidence supports a role for the yeast CCR4-NOT complex in transcriptional elongation. Genetics. 2001;158(2):627–34.
9. Kruk JA, Dutta A, Fu J, Gilmour DS, Reese JC. The multifunctional Ccr4-Not complex directly promotes transcription elongation. Genes Dev. 2011;25(6):581–93. https://doi.org/10.1101/gad.2020911.
10. Collart MA, Panasenko OO. The Ccr4-Not complex. Gene. 2012;492:42–53.
11. Kerr SC, Azzouz N, Fuchs SM, Collart MA, Strahl BD, Corbett AH, et al. The Ccr4-Not complex interacts with the mRNA Export Machinery. PLoS One. 2011;6(3):e18302.
12. Panasenko OO, Somasekharan SP, Villanyi Z, Zagatti M, Bezrukov F, Rashpa R, et al. Co-translational assembly of proteasome subunits in NOT1-containing assemblysomes. Nat Struct Mol Biol. 2019;26(2):110–20. https://doi.org/10.1038/s41594-018-0179-5.
13. Kuzuoğlu-Öztürk D, Bhandari D, Huntzinger E, Fauser M, Helms S, Izaurralde E. mi RISC and the CCR 4– NOT complex silence mRNA targets independently of 43S ribosomal scanning. EMBO J. 2016;35(11):1186–203. https://doi.org/10.15252/embj.201592901.
14. Mathys H, Basquin JÔ, Ozgur S, Czarnocki-Cieciura M, Bonneau F, Aartse A, et al. Structural and Biochemical Insights to the Role of the CCR4-NOT complex and DDX6 ATPase in microRNA repression. Mol Cell. 2014;54(5):751–65. https://doi.org/10.1016/j.molcel.2014.03.036.
15. Tucker M, Valencia-Sanchez MA, Staples RR, Chen J, Denis CL, Parker R. The transcription factor associated Ccr4 and Caf1 proteins are components of the major cytoplasmic mRNA deadenylase in Saccharomyces cerevisiae. Cell. 2001;104(3):377–86. https://doi.org/10.1016/S0092-8674(01)00225-2.
16. Webster MW, Chen YH, Stowell JAW, Alhusaini N, Sweet T, Graveley BR, et al. mRNA deadenylation is coupled to translation rates by the differential activities of Ccr4-Not nucleases. Mol Cell. 2018;70(6):1089–1100.e8.
17. Nousch M, Techritz N, Hampel D, Millonigg S, Eckmann CR. The Ccr4-Not deadenylase complex constitutes the main poly(A) removal activity in C. elegans. J Cell Sci. 2013;126(Pt 18):4274–85. https://doi.org/10.1242/jcs.132936.
18. Lau NC, Kolkman A, van Schaik FMA, Mulder KW, Pijnappel WWWP, Heck AJR, et al. Human Ccr4-Not complexes contain variable deadenylase subunits. Biochem J. 2009;422(3):443–53. https://doi.org/10.1042/BJ20090500.
19. Ito K, Takahashi A, Morita M, Suzuki T, Yamamoto T. The role of the CNOT1 subunit of the CCR4-NOT complex in mRNA deadenylation and cell viability. Protein Cell. 2011;2(9):755–63. https://doi.org/10.1007/s13238-011-1092-4.
20. Bawankar P, Loh B, Wohlbold L, Schmidt S, Izaurralde E. NOT10 and C2orf29/NOT11 form a conserved module of the CCR4-NOT complex that docks onto the NOT1 N-terminal domain. RNA Biol. 2013;10(2):228–44. https://doi.org/10.4161/rna.23018.
21. Meijer HA, Schmidt T, Gillen SL, Langlais C, Jukes-Jones R, De Moor CH, et al. DEAD-box helicase eIF4A2 inhibits CNOT7 deadenylation activity. Nucleic Acids Res. 2019;47(15):8224–38. https://doi.org/10.1093/nar/gkz509.
22. Otsuka H, Fukao A, Tomohiro T, Adachi S, Suzuki T, Takahashi A, et al. ARE-binding protein ZFP36L1 interacts with CNOT1 to directly repress translation via a deadenylation-independent mechanism. Biochimie. 2020;174:49–56. https://doi.org/10.1016/j.biochi.2020.04.010.
23. Dassi E. Handshakes and fights: the regulatory interplay of RNA-binding proteins. Front Mol Biosci. 2017;4:67.
24. Lapointe CP, Preston MA, Wilinski D, Saunders HAJ, Campbell ZT, Wickens M. Architecture and dynamics of overlapped RNA regulatory networks. RNA. 2017;23(11):1636–47. https://doi.org/10.1261/rna.062687.117.
25. Liu L, Ouyang M, Rao JN, Zou T, Xiao L, Chung HK, et al. Competition between RNA-binding proteins CELF1 and HuR modulates MYC translation and intestinal epithelium renewal. Mol Biol Cell. 2015;26(10):1797–810. https://doi.org/10.1091/mbc.E14-11-1500.
26. Plass M, Rasmussen SH, Krogh A. Highly accessible AU-rich regions in 3′ untranslated regions are hotspots for binding of regulatory factors. PLoS Comput Biol. 2017;13(4):e1005460. https://doi.org/10.1371/journal.pcbi.1005460.
27. Piao X, Zhang X, Wu L, Belasco JG. CCR4-NOT Deadenylates mRNA Associated with RNA-induced silencing complexes in human cells. Mol Cell Biol. 2010;30(6):1486–94. https://doi.org/10.1128/MCB.01481-09.

28. Buschauer R, Matsuo Y, Sugiyama T, Chen YH, Alhusaini N, Sweet T, et al. The Ccr4-Not complex monitors the translating ribosome for codon optimality. Science. 2020;368(6488):eaay6912.
29. Vicens Q, Kieft JS, Rissland OS. Revisiting the closed-loop model and the nature of mRNA 5′–3′ communication. Mol Cell. 2018;72:805–12. Cell Press. https://doi.org/10.1016/j.molcel.2018.10.047.
30. Gallie DR. The cap and poly(A) tail function synergistically to regulate mRNA translational efficiency. Genes Dev. 1991; 5(11):2108–16. https://doi.org/10.1101/gad.5.11.2108.
31. Wells SE, Hillner PE, Vale RD, Sachs AB. Circularization of mRNA by eukaryotic translation initiation factors. Mol Cell. 1998; 2(1):135–40. https://doi.org/10.1016/S1097-2765(00)80122-7.
32. Amrani N, Ghosh S, Mangus DA, Jacobson A. Translation factors promote the formation of two states of the closed-loop mRNP. Nature. 2008;453(7199):1276–80. https://doi.org/10.1038/nature06974.
33. Yi H, Park J, Ha M, Lim J, Chang H, Kim VN, et al. Mol Cell. 2018;70(6):1081–1088.e5.
34. Fabian MR, Mathonnet G, Sundermeier T, Mathys H, Zipprich JT, Svitkin YV, et al. Mammalian miRNA RISC Recruits CAF1 and PABP to Affect PABP-Dependent Deadenylation. Mol Cell. 2009;35(6):868–80. https://doi.org/10.1016/j.molcel.2009.08.004.
35. Wang H, Morita M, Yang X, Suzuki T, Yang W, Wang J, et al. Crystal structure of the human CNOT6L nuclease domain reveals strict poly(A) substrate specificity. EMBO J. 2010;29(15):2566–76. https://doi.org/10.1038/emboj.2010.152.
36. Sandler H, Kreth J, Timmers HTM, Stoecklin G. Not1 mediates recruitment of the deadenylase Caf1 to mRNAs targeted for degradation by tristetraprolin. Nucleic Acids Res. 2011;39(10):4373–86. https://doi.org/10.1093/nar/gkr011.
37. Doidge R, Mittal S, Aslam A, Winkler GS. Deadenylation of cytoplasmic mRNA by the mammalian Ccr4-Not complex. In: Biochemical Society Transactions; 2012. p. 896–901.
38. Kahvejian A, Svitkin YV, Sukarieh R, M'Boutchou MN, Sonenberg N. Mammalian poly(A)-binding protein is a eukaryotic translation initiation factor, which acts via multiple mechanisms. Genes Dev. 2005;19(1):104–13. https://doi.org/10.1101/gad.1262905.
39. Cooke A, Prigge A, Wickens M. Translational repression by deadenylases. J Biol Chem. 2010;285(37):28506–13. https://doi.org/10.1074/jbc.M110.150763.
40. Ozgur S, Basquin J, Kamenska A, Filipowicz W, Standart N, Conti E. Structure of a human 4E-T/DDX6/CNOT1 complex reveals the different interplay of DDX6-binding proteins with the CCR4-NOT complex. Cell Rep. 2015;13(4):703–11. https://doi.org/10.1016/j.celrep.2015.09.033.
41. Mishima Y, Fukao A, Kishimoto T, Sakamoto H, Fujiwara T, Inoue K. Translational inhibition by deadenylation-independent mechanisms is central to microRNA-mediated silencing in zebrafish. Proc Natl Acad Sci U S A. 2012;109(4): 1104–9. https://doi.org/10.1073/pnas.1113350109.
42. Djuranovic S, Nahvi A, Green R. miRNA-mediated gene silencing by translational repression followed by mRNA deadenylation and decay. Science. 2012;336(6078):237-40.
43. Bazzini AA, Lee MT, Giraldez AJ. Ribosome profiling shows that miR-430 reduces translation before causing mRNA decay in Zebrafish. Science (80-). 2012;336(6078):233–7.
44. Beilharz TH, Humphreys DT, Clancy JL, Thermann R, Martin DIK, Hentze MW, et al. microRNA-mediated messenger RNA deadenylation contributes to translational repression in mammalian cells. Bähler J, editor. PLoS One. 2009;4(8):e6783.
45. Dimitrova LN, Kuroha K, Tatematsu T, Inada T. Nascent peptide-dependent translation arrest leads to Not4p-mediated protein degradation by the proteasome. J Biol Chem. 2009;284(16):10343–52. https://doi.org/10.1074/jbc.M808840200.
46. Panasenko OO, Collart MA. Presence of Not5 and ubiquitinated Rps7A in polysome fractions depends upon the Not4 E3 ligase. Mol Microbiol. 2012;83(3):640–53. https://doi.org/10.1111/j.1365-2958.2011.07957.x.
47. Villanyi Z, Collart MA. Ccr4-Not is at the core of the eukaryotic gene expression circuitry. Biochem Soc Trans. 2015;43: 1253–8.
48. Timmers HTM, Tora L. Transcript buffering: a balancing act between mRNA synthesis and mRNA degradation. Mol Cell. 2018;72(1):10–7. https://doi.org/10.1016/j.molcel.2018.08.023.
49. Frumkin I, Lajoie MJ, Gregg CJ, Hornung G, Church GM, Pilpel Y. Codon usage of highly expressed genes affects proteome-wide translation efficiency. Proc Natl Acad Sci U S A. 2018;115(21):E4940–9. https://doi.org/10.1073/pnas.1719375115.
50. Hanson G, Coller J. Translation and protein quality control: codon optimality, bias and usage in translation and mRNA decay. Nat Rev Mol Cell Biol. 2018;19:20–30 Nature Publishing Group.
51. Jeacock L, Faria J, Horn D. Codon usage bias controls mRNA and protein abundance in trypanosomatids. Elife. 7. https://doi.org/10.7554/eLife.32496.
52. Presnyak V, Alhusaini N, Chen YH, Martin S, Morris N, Kline N, et al. Codon optimality is a major determinant of mRNA stability. Cell. 2015;160(6):1111–24. https://doi.org/10.1016/j.cell.2015.02.029.
53. Yu CH, Dang Y, Zhou Z, Wu C, Zhao F, Sachs MS, et al. Codon usage influences the local rate of translation elongation to regulate co-translational protein folding. Mol Cell. 2015;59(5):744–54. https://doi.org/10.1016/j.molcel.2015.07.018.
54. Narula A, Ellis J, Taliaferro JM, Rissland OS. Coding regions affect mRNA stability in human cells. RNA. 2019;25(12):1751–64. https://doi.org/10.1261/rna.073239.119.
55. Temme C, Simonelig M, Wahle E. Deadenylation of mRNA by the CCR4-NOT complex in Drosophila: molecular and developmental aspects. Front Genet. 2014;5:143.
56. Wahle E, Winkler GS. RNA decay machines: deadenylation by the Ccr4-not and Pan2-Pan3 complexes. Biochim Biophys Acta. 2013;1829(6–7):561–70. https://doi.org/10.1016/j.bbagrm.2013.01.003.
57. Zheng D, Ezzeddine N, Chen CYA, Zhu W, He X, Shyu A. Bin. Deadenylation is prerequisite for P-body formation and mRNA decay in mammalian cells. J Cell Biol. 2008;182(1):89–101. https://doi.org/10.1083/jcb.200801196.
58. Zubiaga AM, Belasco JG, Greenberg ME. The nonamer UUAUUUAUU is the key AU-rich sequence motif that mediates mRNA degradation. Mol Cell Biol. 1995;15(4):2219–30. https://doi.org/10.1128/MCB.15.4.2219.
59. Wu L, Fan J, Belasco JG. MicroRNAs direct rapid deadenylation of mRNA. Proc Natl Acad Sci U S A. 2006;103(11):4034–9. https://doi.org/10.1073/pnas.0510928103.
60. Van Etten J, Schagat TL, Hrit J, Weidmann CA, Brumbaugh J, Coon JJ, et al. Human pumilio proteins recruit multiple deadenylases to efficiently repress messenger RNAs. J Biol Chem. 2012;287(43):36370–83. https://doi.org/10.1074/jbc.M112.373522.

61. Arvola RM, Chang C-T, Buytendorp JP, Levdansky Y, Valkov E, Freddolino PL, et al. Unique repression domains of Pumilio utilize deadenylation and decapping factors to accelerate destruction of target mRNAs. Nucleic Acids Res. 2019;48(4):1843–71. https://doi.org/10.1093/nar/gkz1187.
62. Weidmann CA, Raynard NA, Blewett NH, Van Etten J, Goldstrohm AC. The RNA binding domain of Pumilio antagonizes poly-adenosine binding protein and accelerates deadenylation. RNA. 2014;20(8):1298–319. https://doi.org/10.1261/rna.046029.114.
63. Miller JE, Reese JC. Ccr4-Not complex: the control freak of eukaryotic cells. Crit Rev Biochem Mol Biol. 2012;47:315–33.
64. Yamada T, Akimitsu N. Contributions of regulated transcription and mRNA decay to the dynamics of gene expression. Wiley Interdiscip Rev RNA. 2019;10(1):e1508. https://doi.org/10.1002/wrna.1508.
65. Bensaude O. Inhibiting eukaryotic transcription: which compound to choose? How to evaluate its activity? Transcription. 2011;2(3):103–8. https://doi.org/10.4161/trns.2.3.16172.
66. Schueler M, Munschauer M, Gregersen LH, Finzel A, Loewer A, Chen W, et al. Differential protein occupancy profiling of the mRNA transcriptome. Genome Biol. 2014;15(1):R15. https://doi.org/10.1186/gb-2014-15-1-r15.
67. Vissers LELM, Kalvakuri S, de Boer E, Geuer S, Oud M, van Outersterp I, et al. De novo variants in CNOT1, a central component of the CCR4-NOT complex involved in gene expression and RNA and protein stability, cause neurodevelopmental delay. Am J Hum Genet. 2020;107(1):164–72. https://doi.org/10.1016/j.ajhg.2020.05.017.
68. Elmén L, Volpato CB, Kervadec A, Pineda S, Kalvakuri S, Alayari NN, et al. Silencing of CCR4-NOT complex subunits affect heart structure and function. Dis Model Mech. 2020;13(7):dmm044727.
69. Thompson MK, Gilbert WV. mRNA length-sensing in eukaryotic translation: reconsidering the "closed loop" and its implications for translational control. Curr Genet. 2017;63(4):613–20. https://doi.org/10.1007/s00294-016-0674-3.
70. Leppek K, Das R, Barna M. Functional 5′ UTR mRNA structures in eukaryotic translation regulation and how to find them. Nat Rev Mol Cell Biol. 2018;19:158–74 Nature Publishing Group.
71. Kuhn M. Building predictive models in R using the caret package. J Stat Softw. 2008;28(5):1–26. https://doi.org/10.18637/jss.v028.i05.
72. Mishima Y, Tomari Y. Codon usage and 3′ UTR length determine maternal mRNA stability in zebrafish. Mol Cell. 2016;61(6):874–85. https://doi.org/10.1016/j.molcel.2016.02.027.
73. Carneiro RL, Requião RD, Rossetto S, Domitrovic T, Palhano FL. Codon stabilization coefficient as a metric to gain insights into mRNA stability and codon bias and their relationships with translation. Nucleic Acids Res. 2019;47(5):2216–28. https://doi.org/10.1093/nar/gkz033.
74. Topisirovic I, Sonenberg N. Distinctive tRNA repertoires in proliferating versus differentiating cells. Cell. 2014;158(6):1238–9.
75. Bornelöv S, Selmi T, Flad S, Dietmann S, Frye M. Codon usage optimization in pluripotent embryonic stem cells. Genome Biol. 2019;20(1):119. https://doi.org/10.1186/s13059-019-1726-z.
76. Guimaraes JC, Mittal N, Gnann A, Jedlinski D, Riba A, Buczak K, et al. A rare codon-based translational program of cell proliferation. Genome Biol. 2020;21(1):44. https://doi.org/10.1186/s13059-020-1943-5.
77. Forrest ME, Pinkard O, Martin S, Sweet TJ, Hanson G, Coller J. Codon and amino acid content are associated with mRNA stability in mammalian cells. Kim YK, editor. PLoS One. 2020;15(2):e0228730.
78. Hanson G, Alhusaini N, Morris N, Sweet T, Coller J. Translation elongation and mRNA stability are coupled through the ribosomal A-site. RNA. 2018;24(10):1377–89. https://doi.org/10.1261/rna.066787.118.
79. Wu Q, Medina SG, Kushawah G, Devore ML, Castellano LA, Hand JM, et al. Translation affects mRNA stability in a codon-dependent manner in human cells. Elife. 2019;8:e45396.
80. Chekulaeva M, Mathys H, Zipprich JT, Attig J, Colic M, Parker R, et al. MiRNA repression involves GW182-mediated recruitment of CCR4-NOT through conserved W-containing motifs. Nat Struct Mol Biol. 2011;18(11):1218–26. https://doi.org/10.1038/nsmb.2166.
81. Meijer HA, Kong YW, Lu WT, Wilczynska A, Spriggs RV, Robinson SW. Translational repression and eIF4A2 activity are critical for microRNA-mediated gene regulation. Science. (80-). 2013;340(6128):82–5.
82. Wilczynska A, Gillen SL, Schmidt T, Meijer HA, Jukes-Jones R, Langlais C, et al. EIF4A2 drives repression of translation at initiation by Ccr4-Not through purine-rich motifs in the 5′UTR. Genome Biol. 2019;20(1):1–21. https://doi.org/10.1186/s13059-019-1857-2.
83. Ingolia NT, Brar GA, Rouskin S, Mcgeachy AM, Weissman JS. The ribosome profiling strategy for monitoring translation in vivo by deep sequencing of ribosome-protected mRNA fragments. Nat Protoc. 2012;7(8):1534–50.
84. Ingolia NT. Genome-wide translational profiling by Ribosome footprinting. Methods Enzymol. 2010;470(C):119–42. https://doi.org/10.1016/S0076-6879(10)70006-9.
85. Love MI, Huber W, Anders S. Moderated estimation of fold change and dispersion for RNA-seq data with DESeq2. Genome Biol. 2014;15(12). https://doi.org/10.1186/s13059-014-0550-8.
86. Zhu A, Ibrahim JG, Love MI. Heavy-Tailed prior distributions for sequence count data: Removing the noise and preserving large differences. Bioinformatics. 2019;35(12):2084–92. https://doi.org/10.1093/bioinformatics/bty895.
87. Geladaki A, Kočevar Britovšek N, Breckels LM, Smith TS, Vennard OL, Mulvey CM, et al. Combining LOPIT with differential ultracentrifugation for high-resolution spatial proteomics. Nat Commun. 2019;10(1):1–15. https://doi.org/10.1038/s41467-018-08191-w.
88. Schwanhäusser B, Gossen M, Dittmar G, Selbach M. Global analysis of cellular protein translation by pulsed SILAC. Proteomics. 2009;9(1):205–9. https://doi.org/10.1002/pmic.200800275.
89. Wolin SL, Walter P. Signal recognition particle mediates a transient elongation arrest of preprolactin in reticulocyte lysate. J Cell Biol. 1989;109(6):2617–22.
90. Arpat AB, Liechti A, De Matos M, Dreos R, Janich P, Gatfield D. Transcriptome-wide sites of collided ribosomes reveal principles of translational pausing. Genome Res. 2020;30(7):985–99. https://doi.org/10.1101/gr.257741.119.
91. Almagro Armenteros JJ, Tsirigos KD, Sønderby CK, Petersen TN, Winther O, Brunak S, et al. SignalP 5.0 improves signal peptide predictions using deep neural networks. Nat Biotechnol. 2019;37(4):420–3. https://doi.org/10.1038/s41587-019-0036-z.
92. Courel M, Clément Y, Bossevain C, Foretek D, Cruchez OV, Yi Z, et al. Gc content shapes mRNA storage and decay in human cells. Elife. 2019;8:1–32. https://doi.org/10.7554/eLife.49708.
93. Hubstenberger A, Courel M, Bénard M, Souquere S, Ernoult-Lange M, Chouaib R, et al. P-body purification reveals the condensation of repressed mRNA regulons. Mol Cell. 2017;68(1):144–157.e5.

94. Rehwinkel JAN, Behm-ansmant I, Gatfield D, Izaurralde E. A crucial role for GW182 and the DCP1 : DCP2 decapping complex in miRNA-mediated gene silencing. RNA. 2005:1640–7. https://doi.org/10.1261/rna.2191905.
95. Chen CYA, Bin SA. Mechanisms of deadenylation-dependent decay. Wiley Interdiscip Rev: RNA. 2011;2:167–83.
96. Ayache J, Bénard M, Ernoult-lange M, Minshall N, Standart N, Matera AG. P-body assembly requires DDX6 repression complexes rather than decay or Ataxin2 / 2 L complexes. Mol Biol Cell. 2015;26(14):2579–95. https://doi.org/10.1091/mbc.E15-03-0136.
97. Minshall N, Kress M, Weil D, Standart N. Role of p54 RNA helicase activity and its c-terminal domain in translational repression, p-body localization and assembly. Mol Biol Cell. 2009;20(9):2464–72. https://doi.org/10.1091/mbc.e09-01-0035.
98. Luo Y, Na Z, Slavoff SA. P-bodies: composition, properties, and functions. Biochemistry. 2018;57(17):2424–31. https://doi.org/10.1021/acs.biochem.7b01162.
99. Ozgur S, Chekulaeva M, Stoecklin G. Human Pat1b connects deadenylation with mRNA decapping and controls the assembly of processing bodies. Mol Cell Biol. 2010;30(17):4308–23. https://doi.org/10.1128/MCB.00429-10.
100. Brengues M, Teixeira D, Parker R. Movement of eukaryotic mRNAs between polysomes and cytoplasmic processing bodies. Science. 2005;310(5747):486–9. https://doi.org/10.1126/science.1115791.
101. Parker R, Sheth U. Review P bodies and the control of mRNA translation and degradation. Mol Cell. 2007;25(5):635–46.
102. Coller J, Parker R. General translational repression by activators of mRNA decapping. Cell. 2005;122(6):875–86. https://doi.org/10.1016/j.cell.2005.07.012.
103. Shih J-W, Wang W-T, Tsai T-Y, Kuo C-Y, Li H-K, Wu Lee Y-H. Critical roles of RNA helicase DDX3 and its interactions with eIF4E/PABP1 in stress granule assembly and stress response. Biochem J. 2012;441(1):119–29. https://doi.org/10.1042/BJ20110739.
104. Räsch F, Weber R, Izaurralde E, Igreja C. 4E-T-bound mRNAs are stored in a silenced and deadenylated form. Genes Dev. 2020;34(11–12):847–860.
105. Temme C, Zhang L, Kremmer E, Ihling C, Chartier A, Sinz A, et al. Subunits of the Drosophila CCR4-NOT complex and their roles in mRNA deadenylation. RNA. 2010;16(7):1356–70. https://doi.org/10.1261/rna.2145110.
106. Uversky VN. Intrinsically disordered proteins and their "Mysterious" (meta)physics. Front Physics. 2019;7:10 Frontiers Media S.A.
107. Uversky VN. The alphabet of intrinsic disorder. Intrinsically Disord Proteins. 2013;1(1):e24684. https://doi.org/10.4161/idp.24684.
108. Riba A, Di Nanni N, Mittal N, Arhné E, Schmidt A, Zavolan M. Protein synthesis rates and ribosome occupancies reveal determinants of translation elongation rates. Proc Natl Acad Sci U S A. 2019;116(30):15023–32. https://doi.org/10.1073/pnas.1817299116.
109. Charneski CA, Hurst LD. Positively charged residues are the major determinants of ribosomal velocity. Malik HS, editor. PLoS Biol. 2013;11(3):e1001508.
110. Thomas PD, Campbell MJ, Kejariwal A, Mi H, Karlak B, Daverman R, et al. PANTHER: a library of protein families and subfamilies indexed by function. Genome Res. 2003;13(9):2129–41.
111. Thomsen MCF, Nielsen M. Seq2Logo: a method for construction and visualization of amino acid binding motifs and sequence profiles including sequence weighting, pseudo counts and two-sided representation of amino acid enrichment and depletion. Nucleic Acids Res. 2012;40(W1):W281–7. https://doi.org/10.1093/nar/gks469.
112. Braun JE, Huntzinger E, Fauser M, Izaurralde E. GW182 proteins directly recruit cytoplasmic deadenylase complexes to miRNA targets. Mol Cell. 2011;44(1):120–33. https://doi.org/10.1016/j.molcel.2011.09.007.
113. Behm-Ansmant I, Rehwinkel J, Doerks T, Stark A, Bork P, Izaurralde E. mRNA degradation by miRNAs and GW182 requires both CCR4 : NOT deadenylase and DCP1 : DCP2 decapping complexes. Genes Dev. 2006:1885–98. https://doi.org/10.1101/gad.1424106.
114. Otsuka H, Fukao A, Funakami Y, Duncan KE, Fujiwara T. Emerging evidence of translational control by AU-rich element-binding proteins. Front Genet. 2019;10(MAY):332.
115. Webster MW, Stowell JA, Passmore LA. RNA-binding proteins distinguish between similar sequence motifs to promote targeted deadenylation by Ccr4-Not. Elife. 2019;8:e40670.
116. Collart MA. Global control of gene expression in yeast by the Ccr4-Not complex. Gene. 2003;313:1–16. https://doi.org/10.1016/S0378-1119(03)00672-3 Elsevier.
117. Basquin J, Roudko VV, Rode M, Basquin C, Séraphin B, Conti E. Architecture of the nuclease module of the yeast ccr4-Not complex: The not1-caf1-ccr4 interaction. Mol Cell. 2012;48(2):207–18. https://doi.org/10.1016/j.molcel.2012.08.014.
118. Burrow DA, Martin S, Quail JF, Alhusaini N, Coller J, Cleary MD. Attenuated codon optimality contributes to neural-specific mRNA decay in Drosophila. Cell Rep. 2018;24(7):1704–12. https://doi.org/10.1016/j.celrep.2018.07.039.
119. Harigaya Y, Parker R. The link between adjacent codon pairs and mRNA stability. BMC Genomics. 2017;18(1):364.
120. Hia F, Yang SF, Shichino Y, Yoshinaga M, Murakawa Y, Vandenbon A, et al. Codon bias confers stability to human mRNAs. EMBO Rep. 2019;20(11):e48220.
121. Gingold H, Tehler D, Christoffersen NR, Nielsen MM, Asmar F, Kooistra SM, et al. A dual program for translation regulation in cellular proliferation and differentiation. Cell. 2014;158(6):1281–92.
122. Vissers LELM, Kalvakuri S, de Boer E, Geuer S, Oud M, van Outersterp I, et al. De novo variants in CNOT1, a central component of the CCR4-NOT complex involved in gene expression and RNA and protein stability, cause neurodevelopmental delay. Am J Hum Genet. 2020;107(1):164–72.
123. Brodsky S, Jana T, Mittelman K, Chapal M, Kumar DK, Carmi M, et al. Intrinsically disordered regions direct transcription factor in vivo binding specificity. Mol Cell. 2020;79(3):459–471.e4.
124. Minezaki Y, Homma K, Kinjo AR, Nishikawa K. Human transcription factors contain a high fraction of intrinsically disordered regions essential for transcriptional regulation. J Mol Biol. 2006;359(4):1137–49. https://doi.org/10.1016/j.jmb.2006.04.016.
125. Ito T, Azumano M, Uwatoko C, Itoh K, Kuwahara J. Role of zinc finger structure in nuclear localization of transcription factor Sp1. Biochem Biophys Res Commun. 2009;380(1):28–32. https://doi.org/10.1016/j.bbrc.2008.12.165.
126. Yamasaki H, Sekimoto T, Ohkubo T, Douchi T, Nagata Y, Ozawa M, et al. Zinc finger domain of Snail functions as a nuclear localization signal for importin β-mediated nuclear import pathway. Genes Cells. 2005;10(5):455–64. https://doi.org/10.1111/j.1365-2443.2005.00850.x.

127. Tyanova S, Temu T, Cox J. The MaxQuant computational platform for mass spectrometry-based shotgun proteomics. Nat Protoc. 2016;11(12):2301–19. https://doi.org/10.1038/nprot.2016.136.
128. Martin M. Cutadapt removes adapter sequences from high-throughput sequencing reads. EMBnet.J. 2012;17(1):2803–9.
129. Fu L, Niu B, Zhu Z, Wu S, Li W. CD-HIT: accelerated for clustering the next-generation sequencing data. Bioinformatics. 2012;28(23):3150–2. https://doi.org/10.1093/bioinformatics/bts565.
130. Dobin A, Davis CA, Schlesinger F, Drenkow J, Zaleski C, Jha S, et al. STAR: Ultrafast universal RNA-seq aligner. Bioinformatics. 2013;29(1):15–21. https://doi.org/10.1093/bioinformatics/bts635.
131. Liao Y, Smyth GK, Shi W. FeatureCounts: an efficient general purpose program for assigning sequence reads to genomic features. Bioinformatics. 2014;30(7):923–30. https://doi.org/10.1093/bioinformatics/btt656.
132. Motulsky HJ, Brown RE. Detecting outliers when fitting data with nonlinear regression - a new method based on robust nonlinear regression and the false discovery rate. BMC Bioinformatics. 2006;7:1–20.
133. Langmead B, Trapnell C, Pop M, Salzberg SL. Ultrafast and memory-efficient alignment of short DNA sequences to the human genome. Genome Biol. 2009;10(3):R25. https://doi.org/10.1186/gb-2009-10-3-r25.
134. Frankish A, Diekhans M, Ferreira AM, Johnson R, Jungreis I, Loveland J, et al. GENCODE reference annotation for the human and mouse genomes. Nucleic Acids Res. 2019;47(D1):D766–73. https://doi.org/10.1093/nar/gky955.
135. Li H, Handsaker B, Wysoker A, Fennell T, Ruan J, Homer N, et al. The Sequence Alignment/Map format and SAMtools. Bioinformatics. 2009;25(16):2078–9. https://doi.org/10.1093/bioinformatics/btp352.
136. Anders S, Pyl PT, Huber W. HTSeq-A Python framework to work with high-throughput sequencing data. Bioinformatics. 2015;31(2):166–9. https://doi.org/10.1093/bioinformatics/btu638.
137. Gillen SL, Giacomelli C, Hodge K, Zanivan S, Bushell M & Wilczynska A Differential regulation of mRNA fate by the human Ccr4-Not complex is driven by coding sequence composition and mRNA localisation Gene Expr Omnibus. (2021). https://www.ncbi.nlm.nih.gov/geo/query/acc.cgi?acc=GSE158619
138. Gillen SL, Giacomelli C, Hodge K, Zanivan S, Bushell M & Wilczynska A Differential regulation of mRNA fate by the human Ccr4-Not complex is driven by coding sequence composition and mRNA localisation Gene Expr Omnibus. (2021). https://www.ncbi.nlm.nih.gov/geo/query/acc.cgi?acc=GSE158141
139. Gillen SL, Giacomelli C, Hodge K, Zanivan S, Bushell M & Wilczynska A Differential regulation of mRNA fate by the human Ccr4-Not complex is driven by coding sequence composition and mRNA localisation Gene Expr Omnibus. (2021). https://www.ncbi.nlm.nih.gov/geo/query/acc.cgi?acc=GSE183148
140. Wilczynska A, Gillen SL, Schmidt T, Meijer HA, Jukes-Jones R, Langlais C, Kopra K, Lu WT, Godfrey JD, Hawley BR, Hodge K, Zanivan SR, Cain K, Le Quesne J, Bushell M. eIF4A2 drives repression of translation at initiation by Ccr4-Not through purine-rich motifs in the 5′UTR. PRIDE Archive. (2019). https://www.ebi.ac.uk/pride/archive/projects/PXD014764
141. Gillen SL, Giacomelli C, Hodge K, Zanivan S, Bushell M & Wilczynska A Differential regulation of mRNA fate by the human Ccr4-Not complex is driven by coding sequence composition and mRNA localisation PRIDE Archive. (2021). https://www.ebi.ac.uk/pride/archive/projects/PXD020305
142. Gillen SL, Giacomelli C, Hodge K, Zanivan S, Bushell M, Wilczynska A. Github; 2021. https://doi.org/10.5281/zenodo.5363113.

Publisher's Note